Ann. Rev. Astron. Astrophys. 1988. 26: 631–86

LARGE-SCALE STRUCTURE IN THE UNIVERSE INDICATED BY GALAXY CLUSTERS

Neta A. Bahcall

Space Telescope Science Institute,[1] Baltimore, Maryland 21218

1. INTRODUCTION

The study of large-scale structure is an attempt to unravel the skeleton of our universe. We try to discover how matter, or at least the luminous matter observed in the form of galaxies and clusters of galaxies, is distributed in space. Early observations suggested that while galaxies show a tendency to cluster into groups and rich clusters on small scales ($\lesssim 20h^{-1}$ Mpc), as expressed statistically by the galaxy correlation function, most of the luminous matter in the Universe is distributed randomly on large scales ($\gtrsim 20h^{-1}$ Mpc). This picture of a relatively "smooth" universal skeleton has been changing quickly and drastically in recent years as new observational data have begun revealing a universe with extensive structure and motion on very large scales of $\sim 100h^{-1}$ Mpc or more. The new data on the large-scale structure have led to major changes in existing theoretical ideas on how galaxies and large-scale structure might have been formed. Several previous models have proven inadequate to explain the new observations, while some new candidate models (e.g. cold dark matter, explosions, cosmic strings) have been suggested and worked out in various degrees of detail. Still, despite the great effort and many ingenious ideas, no single theory for the formation of galaxies and large-scale structure can yet satisfactorily match all the observations.

The reason that large-scale structure is fundamental to our understanding of the Universe is because the structure evolves very slowly with

[1] The Space Telescope Science Institute is operated by the Association of Universities for Research in Astronomy, Inc., for the National Aeronautics and Space Administration.

0066–4146/88/0915–0631$02.00

time. Even for typical velocities of $\sim 10^3$ km s^{-1}, objects can move only $\sim 10h^{-1}$ Mpc within the Hubble time. Therefore, large structures observed today are cosmic fossils of conditions that existed in the early Universe; these fossils record the history of galaxy and structure formation and evolution.

The cosmological principle states that the Universe is homogeneous and isotropic. Observations of galaxies and clusters, however, show inhomogeneities and structure on all scales studied so far. The Universe is clumped on the scales of galaxies (kiloparsecs), clusters (megaparsecs), and very large superclusters (tens of megaparsecs or more, comparable to the largest scale of current samples). When does the Universe become homogeneous? How does the clumpy distribution of the luminous matter fit with the highly isotropic distribution of the microwave background radiation on the largest scales? The answers are not yet known.

The classic method of investigating structure in the Universe is to observe the spatial distribution of galaxies. Extensive surveys of thousands of galaxy redshifts are needed in order to cover large enough volumes and scales. Galaxy redshift surveys have been carried out by several groups (see review papers by Oort 1983, Chincarini & Vettolani 1987, and Rood 1988; also Gregory & Thompson 1978, Gregory et al. 1981, Davis et al. 1982; Giovanelli et al. 1986, de Lapparent et al. 1986, da Costa et al. 1988).

A different approach is emphasized in this review: using the high-density peaks of the galaxy distribution, i.e. the rich clusters of galaxies, as tracers of the large-scale structure. Much as the mountain peaks trace mountain chains on Earth, so too do the rich clusters, with their low space density and large mean separation, serve as an efficient tracer of the largest scale structures. Recent results, summarized in this review, show that clusters do indeed provide an efficient and effective tracer of the large-scale structure of the Universe.

Galaxy and cluster maps of the Northern Hemisphere to $z \lesssim 0.15$ are compared in Figures 1 and 2 [Shane & Wirtanen's (1967) galaxy map and Abell's (1958) rich cluster map, respectively]. The clumped distribution is apparent in both maps. While $\sim 10^6$ galaxies cover the mapped volume, only ~ 500 rich clusters highlight the structure in the same volume of space.

The main observational data placing constraints on the large-scale structure are the following:

1. Rich clusters trace the large-scale structure to $\sim 100h^{-1}$ Mpc scale, revealing strong clustering of clusters to these scales. These results are expressed in terms of superclusters of clusters, or by the cluster-cluster correlation function $\xi_{cc}(r)$, which, for Abell clusters of richness ≥ 1, is

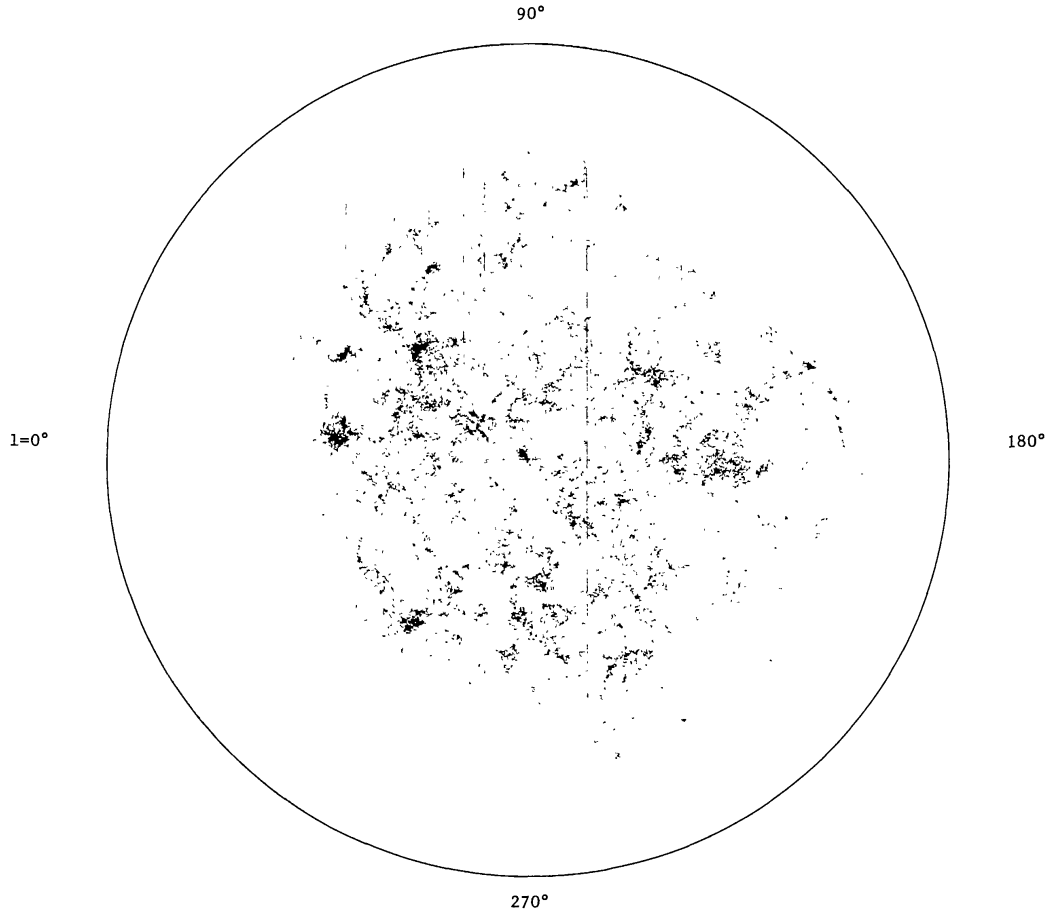

Figure 1 A map of the galaxy distribution in the Northern Hemisphere (to 19^m) from the Shane & Wirtanen (1967) counts (Soneira & Peebles 1978).

unity at approximately $25h^{-1}$ Mpc and remains positive out to $\sim 100h^{-1}$ Mpc (e.g. Bahcall & Soneira 1983). Associated velocities of $\sim 10^3$ km s^{-1} may also be suggested (Bahcall et al. 1986).

2. On a similar scale, the recently reported "bulk motion" of ~ 600 km s^{-1} relative to the microwave background of the sphere of galaxies and clusters around us within $\sim 30h^{-1}$ Mpc (Rubin et al. 1976, Burstein et al. 1986, Collins et al. 1986, Dressler et al. 1987, Aaronson & Mould 1988).
3. Galaxy redshift surveys revealing netlike or spongy structures and voids to scales of $\sim 100h^{-1}$ Mpc (Gregory & Thompson 1978, Gregory et al. 1981, Chincarini et al. 1981, Davis et al. 1982, Giovanelli & Haynes 1982, Oort 1983, Giovanelli et al. 1986, Tully 1987a, de Lapparent et al. 1986, da Costa et al. 1988, Rood 1988).
4. Upper limits to the temperature fluctuations in the microwave background, $\Delta T/T$, on various angular scales (1° corresponding to $\sim 100h^{-1}$

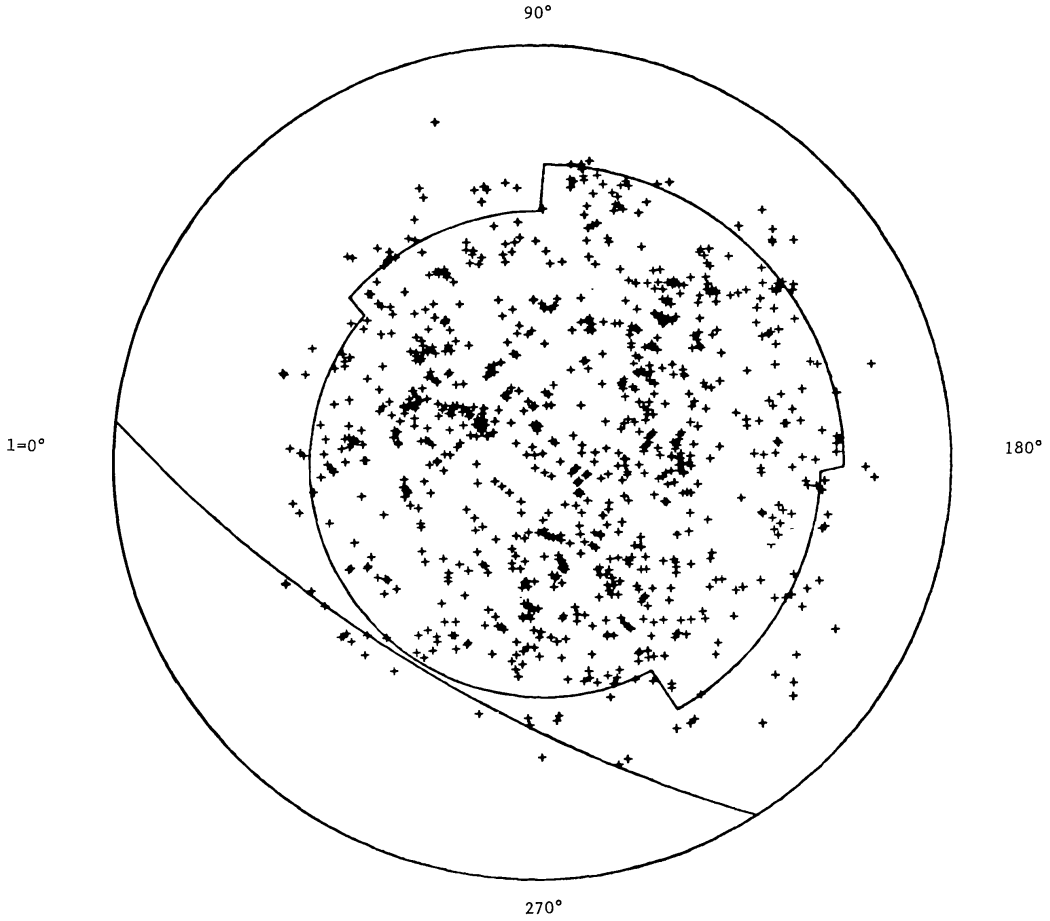

Figure 2 A map of Abell's cluster distribution in the Northern Hemisphere to distance group $D \leq 5$. The inner contour indicates the completeness limit of the statistical sample (Section 2). The map is plotted to the same scale as the galaxy map of Figure 1 and corresponds approximately to the same depth. A comparison of the galaxy and cluster maps (Figures 1, 2) indicates that the clusters and galaxies generally trace the same structure.

Mpc) (e.g. Uson & Wilkinson 1984, Davies et al. 1987, Lasenby 1988, Readhead 1988, Strukov et al. 1988).

5. The clustering of high-redshift objects, such as quasars (Kruszewski 1986, Zhou et al. 1986, Shaver 1988), Lα clouds (Sargent 1988), and high-redshift galaxies (Koo & Kron 1987).

In this paper I review the current results of studies using rich clusters of galaxies to trace the large-scale structure of the Universe. I describe both general statistical analyses, such as the cluster correlation function, as well as specific studies of superclusters and their properties.

For a previous review paper on *superclusters*, see Oort (1983). A review paper on *voids* is presented in this volume by Rood (1988).

I use a Hubble constant of $H_0 = 100h$ km s^{-1} Mpc^{-1} throughout this paper.

2. CATALOGS OF GALAXY CLUSTERS

In order to use rich galaxy clusters as tracers of the large-scale structure in the Universe, a complete sample of clusters over a large volume of space is required. I describe below the available catalogs of rich clusters of galaxies. The clusters in these catalogs were used as tracers, with different techniques employed, as discussed in the sections that follow.

Three extensive catalogs of rich clusters of galaxies are available: The Abell (1958) catalog of rich clusters; the "Catalog of Galaxies and Clusters of Galaxies" by Zwicky et al. (1961–1968); and the catalog of clusters by Shectman (1985) determined from the Shane & Wirtanen (1967) galaxy counts. Abell and Zwicky both identified clusters as density enhancements on the Palomar Sky Survey plates, but they used quite different selection criteria for the inclusion of clusters in their catalogs. Shectman (1985) identified clusters from the Shane & Wirtanen (1967) galaxy counts, using still another selection algorithm of density enhancement. I summarize below the selection algorithms and the main properties of these catalogs.

The obvious next step is to use a completely automated procedure of identifying clusters by computer algorithms that search data tapes of computer-scanned images. Such "objective" catalogs are being prepared by several groups (e.g. Maddox et al. 1988). A complete sample of X-ray-selected rich clusters of galaxies, which will be available in a few years from new X-ray surveys, will provide another objective sample of clusters that can be used to trace the large-scale structure.

2.1 *The Abell Catalog*

The Abell (1958) catalog of rich clusters of galaxies contains a total of 2712 clusters that are the richest, densest clusters found on the Palomar Sky Survey plates and are identified by a well-defined set of selection criteria. Of these rich clusters, 1682 constitute Abell's complete statistical sample; they are distributed over 4.26 steradians of the sky and satisfy restrictive selection criteria. The Abell criteria are summarized as follows: (*a*) A cluster must contain at least 50 members, after proper correction for background, in the magnitude range m_3 to m_3+2, where m_3 is the magnitude of the third brightest galaxy; (*b*) the $\gtrsim 50$ members should be contained within a circle of radius $1.5h^{-1}$ Mpc around the center of the cluster (corresponding to the Abell radius $R_A = 1.7'/z = 1.5h^{-1}$ Mpc, where z is the cluster redshift); (*c*) the cluster redshift z should be in the range $0.02 \lesssim z \lesssim 0.20$; and (*d*) the cluster should lie north of declination $-27°$ and within the region of complete identification given in Table 1 of Abell (1958). The clusters' redshifts are estimated by Abell from the magnitude of the tenth brightest galaxy in the cluster, m_{10}. For each cluster

the catalog lists the cluster position on the sky; m_{10}; the distance group D (estimated from m_{10}); and the richness classification R. (The latter is related to the number of member galaxies brighter than m_3+2 and located within $R_A = 1.5h^{-1}$ Mpc around the cluster center. This population is corrected for a background count in a nearby field.)

The 1682 rich clusters in the statistical sample belong to distance groups $D = 1$ through 6 and have richness classes of $R = 1$ through 5. These richness classes correspond to galaxy richness counts that range from 50 to over 300 members (as defined above); the less populated (poorer) clusters are much more numerous than the more richly populated ones. The distribution of clusters in the statistical sample among distance groups and richness classes is shown in Table 1.

The full list of 2712 clusters is larger than the 1682 clusters in the statistical sample mostly because of the poorer $R = 0$ clusters (with 30 to 49 members), which are not part of the statistical sample. (They are more easily missed at large distances and are therefore incomplete.) In addition, the full list includes some clusters at lower latitude than the boundary of the statistical sample, as well as clusters with estimated redshifts outside the range of the statistical sample.

Table 1 Distribution of Abell clusters with distance and richness[a]

Distance distribution			Richness distribution		
D	$\langle z_{est}\rangle$	$N_{cl}(R \geq 1)$	R	N_{gl}	N_{cl}
1	0.0283	9	(0)	(30–49)	($\gtrsim 10^3$)[b]
2	0.0400	2	1	50–79	1224
3	0.0577	33	2	80–129	383
4	0.0787	60	3	130–199	68
5	0.131	657	4	200–299	6
6	0.198	921	5	≥ 300	1
Total		1682	Total ($R \geq 1$)		1682

Complete redshift sample (see Section 3)		Distant projected sample (see Section 3)
$D \leq 4$		$D = 5+6$
N_{cl} (total)	104	1547
N_{cl} ($b \geq 30°$)	71	984
N_{cl} ($b \leq -30°$)	33	563
N_{cl} ($R = 1$)	82	1125
N_{cl} ($R \geq 2$)	22	422

[a] Notation: D = distance group; $\langle z_{est}\rangle$ = estimated redshift; N_{cl} = number of clusters; R = richness class; N_{gl} = number of galaxies (cluster population).
[b] $R = 0$ clusters are not part of the statistical sample.

Redshifts for all clusters in Abell's statistical nearby sample of distance class $D \leq 4$ ($z \lesssim 0.1$) were recently measured by Hoessel et al. (1980). This complete redshift sample includes 104 clusters at $D \leq 4$ that are of richness class $R \geq 1$ and are located at high Galactic latitude (as specified in Abell's Table 1 plus the requirement of $|b| \geq 30°$). This complete nearby redshift sample was used extensively in tracing the large-scale structure in space (Sections 3.2.1, 6, and 8). A somewhat larger sample of 175 clusters that include $R = 0$ clusters with measured redshifts, for the same distance groups $D \leq 4$, was also used in several studies. Two selection effects within this bright nearby sample were observed and quantified by Bahcall & Soneira (1983): an observed decrease of cluster density at low latitudes (to $b \sim 30°$), arising probably from obscuration and confusion with high-density regions of stars; and a decrease of cluster spatial density near the redshift limit of the sample, as expected from the uncertainties in the magnitude limit of the Abell distance group. Both of these selection effects, however, can be easily corrected for when using the sample for statistical purposes.

An estimate of the completeness limit of this nearby sample obtained by comparison with X-ray emission from the clusters suggests a reasonably high level of completeness (see Section 3.3).

The mean space density of rich clusters ($R \geq 1$) is observed to be $6 \times 10^{-6} h^3$ Mpc^{-3}, uncorrected for obscuration. When corrected for the latter, the spatial density of $R \geq 1$ clusters increases to $\sim 10^{-5} h^3$ Mpc^{-3}. The density decreases rapidly with increasing richness. The luminosity function of clusters was determined by Bahcall (1979).

A map showing the surface distribution of Abell clusters (Northern Hemisphere, $D \leq 5$) is shown in Figure 2. The distribution is similar to that seen in comparable galaxy maps and shows a highly clumped distribution of clusters. The clumped distribution, analyzed quantitatively in Sections 3 and 6, reflects the large-scale structure of the Universe as traced by galaxy clusters.

An extension of the Abell catalog to the Southern Hemisphere, which was started by Abell before his death, was recently completed by Abell et al. (1988).

2.2 *The Zwicky Catalog*

The Zwicky et al. (1961–68) "Catalog of Galaxies and Clusters of Galaxies" contains over 30,000 galaxies brighter than 15.7^m identified on the Palomar Sky Survey plates and 9700 clusters of galaxies visible to the limit of the plates ($m \simeq 20$). The criteria for including a cluster in the Zwicky catalog are less strict than Abell's. These criteria are the following: (*a*) The cluster must contain at least 50 galaxies in the magnitude range m_1 to

$m_1 + 3$, where m_1 is the magnitude of the brightest galaxy; (*b*) these galaxies must lie within the cluster's contour, defined as the isopleth where the projected density of galaxies is about twice that of the neighboring field; (*c*) no limit on the cluster redshift is specified, but aggregates such as the Virgo cluster (which cover very large areas of the sky) are not included in the contour maps; and (*d*) the clusters must lie north of declination $-3°$ and within the areas given in the introduction to Volume 6 of the catalog.

Zwicky classifies cluster distances according to estimated redshifts (from brightness and apparent size of member galaxies): near clusters ($z \lesssim 0.05$), medium distant ($z \simeq 0.05$–0.10), distant ($z \simeq 0.10$–0.15), very distant ($z \simeq 0.15$–0.2), and extremely distant ($z \gtrsim 0.2$).

Cluster population (or richness) is defined by Zwicky as the number of galaxies visible on the red Palomar Sky Survey plate, corrected for the mean field count, that are located within the isopleth of twice the field density. Because of the boundary at twice the field density, and the count to the plate limit, Zwicky's populations depend systematically on the cluster redshift (unlike the absolute intrinsic richness classification of Abell).

The Zwicky catalog contains systems that are less rich than those of Abell, and hence it has many more clusters. Zwicky clusters also differ in size from Abell's; Zwicky clusters are mostly larger, lower density systems that may contain multiple dense clumps within them. These differences in cluster properties for the two catalogs arise mainly from the different criteria used in the identification process.

2.3 *The Shectman Catalog*

The Shane & Wirtanen (1967) counts of galaxies using the Lick Observatory astrographic survey include about 10^6 galaxies brighter than 19^m at declinations $\delta > -22.5°$. A large number of clusters, i.e. high-density regions of galaxies, are easily recognized in these counts (see Figure 1). Shectman (1985), using an automated procedure, has identified a sample of 646 clusters of galaxies based on the Shane-Wirtanen counts in 10′ bins. The clusters are located at Galactic latitudes $|b| \geq 40°$ and declinations $\delta > -22.5°$. The selection was based on local density maxima above a given threshold value, after lightly smoothing the data to reduce the effect of the sampling grid.

A selected threshold value of five galaxy counts per bin was used by Shectman for the catalog; this threshold is considerably higher than the tail of the random (background) distribution of galaxy counts, which has a median of 1.3 galaxies per bin. Because of the smoothing, a minimum of 20 galaxies must be counted by Shane & Wirtanen to 19^m in order to result in a detection of a cluster. The above threshold of five galaxies

succeeds in detecting 70% of Abell's $D \leq 4$ clusters and 10% of the $D = 5$ clusters. A threshold of about 3.5–4 galaxy counts per bin appears to identify all of Abell's $D \leq 4$ clusters and still be well out on the tail of the random distribution.

The Shectman procedure selects clusters that are considerably poorer than the Abell $R \geq 1$ cluster (the latter having ≥ 50 members brighter than m_3+2). The mean number density of the Shectman clusters is thus much higher than the density of the Abell clusters (see below). It is therefore expected that only a fraction of the Shectman clusters will also be clusters in the Abell catalog. Shectman finds that 40% of his clusters are members of the Abell catalog.

Redshift measurements of a complete subsample of 112 Shectman clusters in the south yield a redshift distribution (and thus depth) similar to the clusters in the $D \leq 4$ Abell sample. The implied space density of the Shectman clusters is therefore about 6 times higher than the space density of the Abell $R \geq 1$ clusters.

3. THE CLUSTER CORRELATION FUNCTION

3.1 *Introduction*

The spatial distribution of rich clusters of galaxies and the clustering properties of clusters have been the subject of considerable interest over the past two decades, with a wide range of claims as to the nature and properties of such clustering. Since rich clusters can be used rather efficiently in surveying the structure in large volumes of space, they have recently become an important tool in tracing the large-scale structure of the Universe.

The Abell (1958) catalog of rich clusters has been analyzed by many investigators (e.g. Abell 1958, 1961, Hauser & Peebles 1973, Rood 1976, Bahcall & Soneira 1983, 1984, Klypin & Kopylov 1983, Bahcall et al. 1986, Shvartsman 1988, Kalinkov et al. 1985, Batuski & Burns 1985a, Tully 1986, and references therein) using different techniques in an attempt to determine the spatial distributions of rich clusters. Abell (1958. 1961) found that the surface distribution of the clusters in his statistical sample (see Section 2) was highly nonrandom and reported evidence suggesting the existence of superclusters; Bogart & Wagoner (1973), Hauser & Peebles (1973), and Rood (1976) (see also references therein) also found, using nearest-neighbor distributions and/or angular correlation functions, strong evidence for superclustering among the Abell clusters. The studies dealt primarily with the surface distribution of clusters and, in some cases, used approximate estimates for cluster redshifts. More recently, Bahcall & Soneira (1983, 1984) and, independently, Klypin & Kopylov (1983)

used redshift measurements of complete samples of clusters to determine directly the spatial distribution of rich clusters. The results, discussed in more detail below, indicate that rich clusters of galaxies cluster very strongly in space, forming clusters of clusters of galaxies, or superclusters (see also Section 6). The clustering strength of clusters was observed to be much higher than the clustering strength of galaxies. The clustering or correlation scale for rich clusters was found to be about five times larger than the correlation scale of galaxies. Similar investigations followed thereafter (see below), all yielding consistent results. Since these results provide strong constraints on models for the formation and evolution of galaxies and structure, I review in this section the findings of recent investigations of the clustering of clusters, using various catalogs and methods.

The correlation function (Limber 1953, Peebles 1980a) is one of the best statistical tools to measure quantitatively the clustering of objects in a sample, yielding both clustering strength and extent. The joint probability $dP(\theta)$ of finding two objects in a sample separated by an angle θ and within solid angles $d\Omega_1$ and $d\Omega_2$ is written as

$$dP(\theta) = N^2[1+w(\theta)]d\Omega_1 d\Omega_2, \qquad 1.$$

where $w(\theta)$ is the two-point angular correlation function and N is the surface number density of objects in the sample. The two-point angular correlation function thus describes, as a function of angular scale, the *net* projected pair clustering of objects on the sky *above* that expected from a random distribution.

Similarly, the spatial correlation function $\xi(r)$ is defined by the joint probability $dP(r)$ of finding two objects separated by a distance r and within volume elements dV_1 and dV_2, such that

$$dP(r) = n^2[1+\xi(r)]dV_1 dV_2, \qquad 2.$$

where n is the space density of objects in the sample. The correlations are therefore zero for a random distribution of points and are positive for a clumped distribution on the relevant clumping scale.

3.2 *Cluster Correlations*

3.2.1 ABELL CLUSTERS The two-point spatial correlation function of clusters, $\xi_{cc}(r)$, was determined by Bahcall & Soneira (1983; hereinafter BS83) using Abell's (1958) statistical sample of rich clusters of galaxies of distance class $D \leq 4$ ($z \lesssim 0.1$), with redshifts for all clusters reported by Hoessel et al. (1980). (For properties of the Abell catalog, see Section 2.) This sample includes all 104 Abell clusters at $D \leq 4$ that are of richness class $R \geq 1$ and are located at high Galactic latitude ($|b| \geq 30°$). A summary of the sample properties and its division into distance and richness

classes, as well as into hemispheres, is presented in Table 1 and BS83. Also listed in Table 1 and BS83 are properties of the much larger and deeper $D = 5+6$ statistical sample ($z \lesssim 0.2$) that includes 1547 clusters. While only a small fraction of the redshifts are measured for this sample, it was used, because of its much larger number of clusters, in various comparison tests to strengthen and confirm the results obtained from the $D \leq 4$ sample.

The frequency distribution $F(r)$ for all pairs of clusters with separation r in the sample was determined. In order to minimize the influence of selection effects on the determination of $\xi(r)$, a set of 1000 random catalogs was constructed, each containing 104 clusters randomly distributed within the angular boundaries of the survey region but with the same selection functions in both redshift, $n(z)$, and latitude, $P(b)$, as the Abell redshift sample. The frequency distribution of cluster pairs was determined in both the real and random catalogs, and the results were then compared. This procedure ensures that the selection effects and boundary conditions will affect the data and random catalogs in the same manner.

The spatial correlation function was determined from the relation

$$\xi_{cc}(r) = F(r)/F^{R}(r) - 1, \qquad 3.$$

where $F(r)$ is the observed frequency of pairs in the Abell sample, and $F^{R}(r)$ is the corresponding frequency of random pairs (as determined by the ensemble average frequency of the 1000 random catalogs). An ensemble average random frequency is used in order that $\xi(r)$ not be affected by the fluctuations present in any particular realization of a single random sample. The correlation function was evaluated for various cases, including (*a*) no selection function in latitude [i.e. $P(b) = 1$]; (*b*) full selection function in latitude; (*c*) Northern and Southern Hemispheres treated separately; and (*d*) high- and low-latitude zones ($|b| > 50°$ and $|b| \leq 50°$) treated separately, each with its observed $n(z)$ [and $P(b)$] selection function.

The resulting correlation function is presented in Figure 3. Strong spatial correlations are observed at separations $\lesssim 25h^{-1}$ Mpc. Weaker correlations are observed to larger separations of at least $\sim 50h^{-1}$ Mpc, and possibly $\sim 100h^{-1}$ Mpc, where $\xi_{cc} \sim 0.1$; beyond $150h^{-1}$ Mpc, no statistically significant correlations are observed in the present sample.

The correlation function of Figure 3 can be well approximated by a single power-law relation of the form $\xi_{cc}(r) = 300r^{-1.8}$ for $5 \lesssim r \lesssim 150h^{-1}$ Mpc. The function is smooth, with little scatter at $r \lesssim 50h^{-1}$ Mpc. At $r > 50h^{-1}$ Mpc, the scatter and uncertainties increase, but weak correlations of order 0.2 are still detected at these very large separations. When corrected for velocity broadening among clusters, the intrinsic rich ($R \geq 1$) cluster correlation function was determined by Bahcall & Soneira to be (BS83)

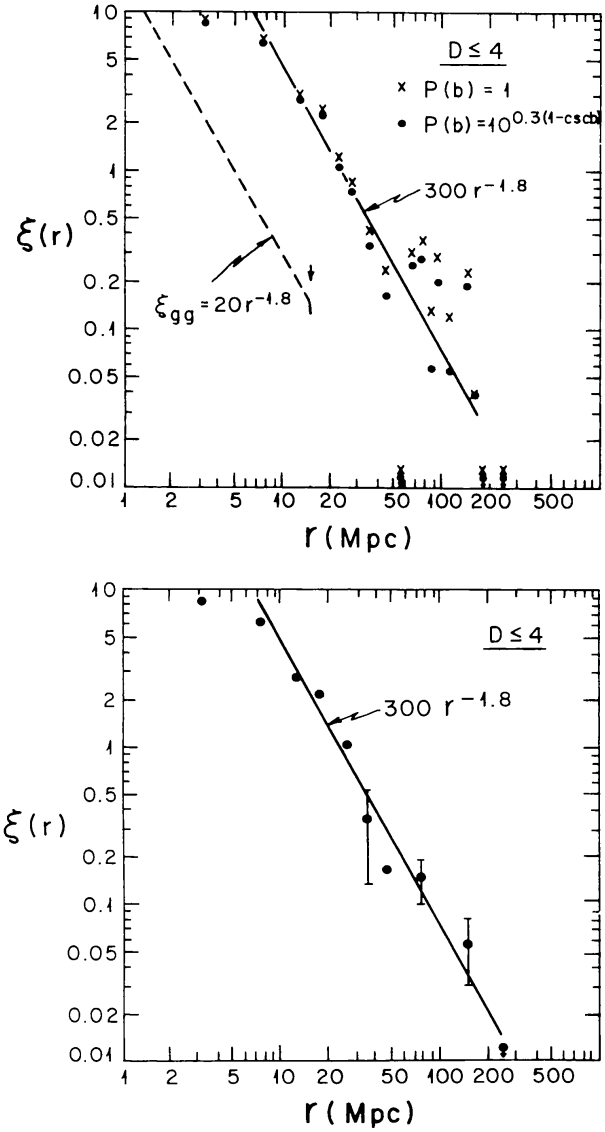

Figure 3 (*Top*) The spatial correlation function of the $D \leq 4$ Abell cluster sample (BS83). [Crosses refer to no correction for latitude selection function; dots refer to the full correction of $P(b)$.] The solid line is the best-fit -1.8 power law to the data. The dashed line is the galaxy-galaxy correlation function of Groth & Peebles (1977). (*Bottom*) Same as (*top*) but plotted in larger bins at large separations.

$$\xi_{cc}(r) = 360r^{-1.8} = (r/26)^{-1.8}, \qquad r \lesssim 100h^{-1}\ \text{Mpc}. \tag{4.}$$

In comparison, the correlation function of galaxies is given by (Groth & Peebles 1977, Davis & Peebles 1983)

$$\xi_{gg}(r) = 20r^{-1.8} = (r/5)^{-1.8}, \qquad r \lesssim 20h^{-1}\ \text{Mpc}. \tag{5.}$$

The rich cluster correlation function has the same shape and slope as those of the galaxy correlation function, but it is considerably stronger at

any given scale (by a factor of ~ 18) than the correlation function of galaxies. The cluster correlations also extend to greater separations than the scales observed in the galaxy correlations. The cluster correlation scale length, i.e. the scale at which the correlation function is unity, is $r_0 \simeq 26h^{-1}$ Mpc (Equation 4), as compared with $r_0 \simeq 5h^{-1}$ Mpc for galaxies. The extent of the rich cluster correlation function beyond the reported $\sim 15h^{-1}$ Mpc break in the galaxy correlation function (Groth & Peebles 1977) suggests the existence of large-scale structure in the Universe ($\gtrsim 15h^{-1}$ Mpc). While the reason for the strong increase of correlation strength and scale from galaxies to clusters is still a theoretical challenge, some possible explanations are discussed in Sections 5 and 9. The cluster correlation function determined above places constraints on models for the formation of galaxies and structure (see Section 9).

In order to ensure that the spatial correlation function is not due to some special peculiarities in the nearby $D \leq 4$ sample, Bahcall & Soneira (BS83) carried out several tests that are discussed below.

First, the angular correlation function of the much larger and deeper $D = 5+6$ sample (1547 $R \geq 1$ clusters to $z \lesssim 0.2$) was determined and compared with that expected from the spatial correlation function above (Equation 4), as well as from the expected scaling law (Peebles 1980a) of the $D \leq 4$ angular correlation function. The angular correlation functions of the nearby $D \leq 4$ and distant $D = 5+6$ samples are determined to be (BS83)

$$w_{D\leq 4}(\theta) \simeq 3\theta^{-1}, \qquad 0.^{\circ}5 \lesssim \theta \lesssim 25^{\circ}, \tag{6.}$$

$$w_{D=5+6}(\theta) \simeq 0.8\theta^{-1}, \qquad 0.^{\circ}2 \lesssim \theta \lesssim 14^{\circ}. \tag{7.}$$

The angular correlations scale as expected from the scaling law applied to their respective distances. A comparison of the scaled functions is shown in Figure 4. If the correlations were mainly due to patchy obscuration or other omissions by Abell, the (observed) scaling would not be expected. The scaling agreement indicates that any possible projection biases in the catalog (e.g. Sutherland 1988) are rather small and do not significantly affect the correlation results (see Bahcall 1988b, Dekel 1988). The reduced correlation scale suggested by Sutherland may result from overcorrecting the actual correlation power on large scales. A comparison of the $D = 5+6$ angular function with that expected from the spatial correlation function of Equation (4), when integrated over the relevant redshift distribution, is shown in Figure 5. The agreement between the $D \leq 4$ and $D = 5+6$ functions is excellent. This agreement indicates that the $D \leq 4$ redshift sample is a fair sample of the much larger sample, and that the observed correlations represent real correlations of clusters in space. The scaling

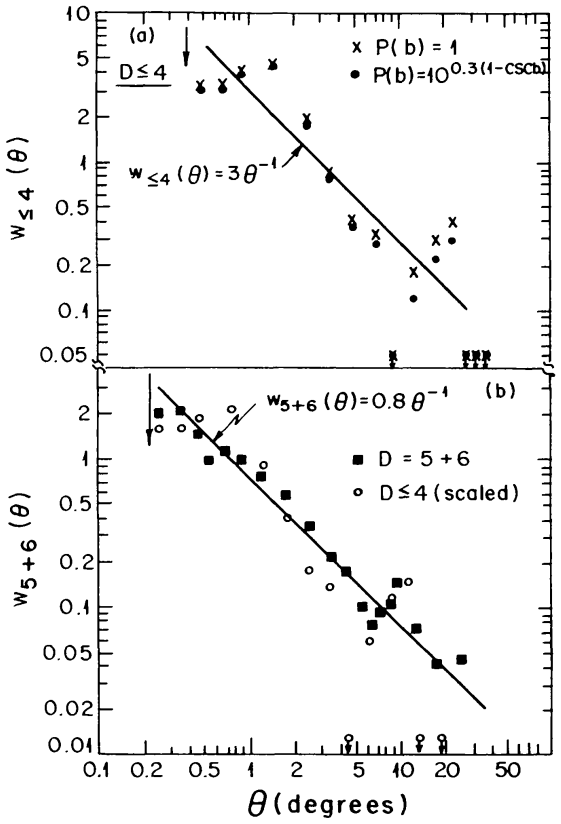

Figure 4 (*a*) The angular correlation function of the $D \leq 4$ Abell cluster sample (BS83). (*b*) The angular correlation function of the deep $D = 5+6$ sample (squares). Open circles are the angular correlation function of the $D \leq 4$ sample (Figure 4*a*) scaled by the standard scaling law of an intrinsic spatial correlation using the distance ratio of the two samples (Section 3). (Correlations of $\lesssim 0.05$ are rather uncertain.) The position of the mean Abell radius is indicated by the arrow.

law of the angular functions was also studied by Hauser & Peebles (1973), who reached similar conclusions with regard to the reality of the intrinsic correlations.

Second, the angular correlation function was compared with the pure redshift (i.e. line-of-sight) correlations of the clusters. If the correlations were mostly due to patchy obscuration on the sky or other similar biases, no extensive redshift correlations would be expected. It is observed (BS83) that the projected and redshift correlations are consistent with each other, further strengthening the reality of the correlations.

Third, the angular correlation function of the $D = 5+6$ sample was determined in different regions of the sky, yielding consistent results within the uncertainties (see Figure 6).

These tests, and those listed in Section 3.3 below, suggest that the observed cluster correlation function is mostly due to physical clustering of rich clusters of galaxies that extends to large scales.

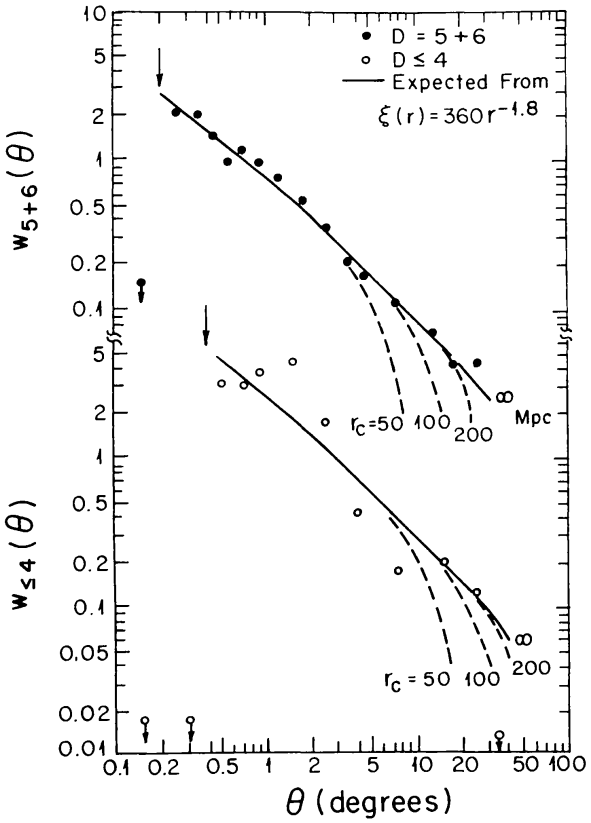

Figure 5 The curves represent the angular correlation function expected from an intrinsic cluster spatial function given by $\xi(r) = 360r^{-1.8}$ for $r \leq r_c$ (Equation 4), and the sample selection function with redshift $n(z)$ (BS83). The top represents the expectation for the $D = 5+6$ Abell sample, and the bottom, the expectation for the $D \leq 4$ sample. Different cutoffs r_c of the intrinsic spatial function are marked. The expected curves are compared with the observed angular correlation functions of the $D = 5+6$ (dots) and $D \leq 4$ (circles) samples. The position of the mean Abell radius, below which no pairs exist, is marked by the arrow for each sample (Section 3.2).

Since the correlation strength appears to increase from galaxies to clusters, Bahcall & Soneira also investigated whether a similar trend is observed between the correlation function of poor and rich clusters. The angular correlation functions of different richness classes ($R = 1$ and $R \geq 2$) were determined for the large $D = 5+6$ sample (1125 $R = 1$ clusters, 422 $R \geq 2$ clusters). The amplitude of the correlation function was found to be strongly dependent on cluster richness, with richer clusters ($R \geq 2$) showing stronger correlations by a factor of ~ 3 as compared with the poorer ($R = 1$) clusters. The results are shown in Figure 7. Both richness classes exhibit the same power-law shape correlation function as observed in the total sample; they satisfy

$$w_{5+6}(\theta) \simeq 0.7\theta^{-1}, \qquad R = 1, \qquad 8.$$

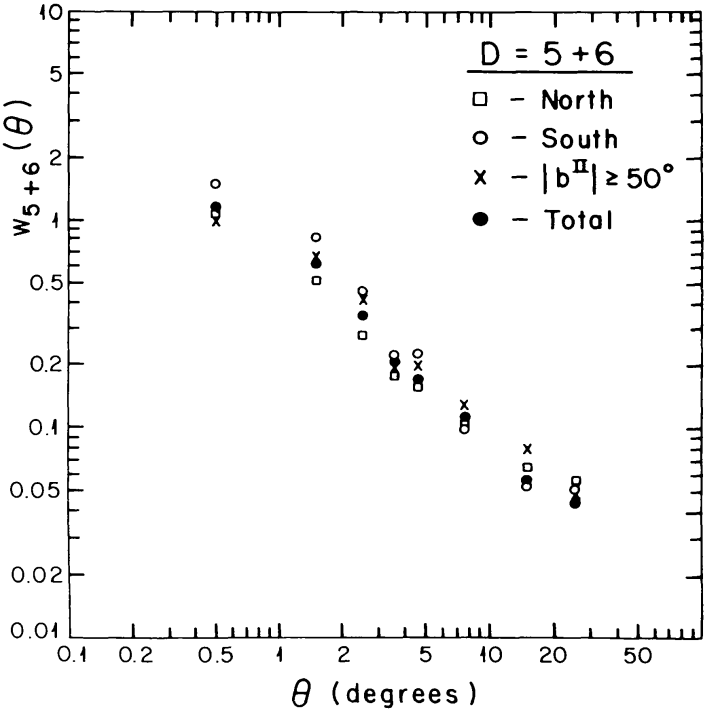

Figure 6 The angular correlation function of the $D = 5+6$ Abell cluster sample for different zones: Northern Hemisphere (squares); Southern Hemisphere (circles); high latitude, $|b^{II}| \geq 50°$ (crosses); and the total sample (dots). (A very strong south-polar apparent supercluster increases somewhat the southern correlations at small separations.) Other zones of low latitude ($|b^{II}| = 30$–$50°$) and different longitudes yield similar results (BS83).

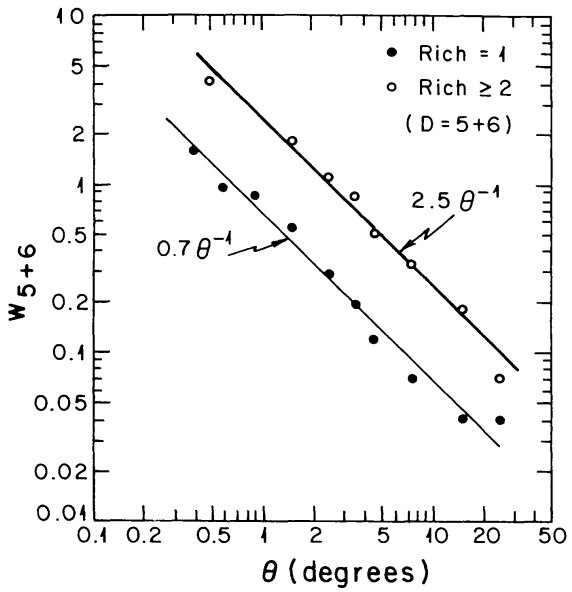

Figure 7 The angular correlation function of richness 1 and richness ≥ 2 Abell clusters in the $D = 5+6$ sample (BS83).

$$w_{5+6}(\theta) \simeq 2.5\theta^{-1}, \qquad R \geq 2. \tag{9.}$$

The implied spatial correlation can then be represented by

$$\xi_{cc}(r) \simeq (r/24)^{-1.8}, \qquad R = 1, \tag{10.}$$

$$\xi_{cc}(r) \simeq (r/48)^{-1.8}, \qquad R \geq 2. \tag{11.}$$

The amplitude of the total ($R \geq 1$) correlation function is dominated by the lower amplitude of the poorer, but more numerous, $R = 1$ clusters. Figure 8 shows the dependence of the correlation function on the richness of the system, from single galaxies to poor and rich clusters, as suggested by BS83 (see also Section 3.5 for a more updated richness dependence). The correlations become stronger with increasing richness (or luminosity) of the system, suggesting that the correlation function depends upon richness. The galaxy-cluster cross-correlation function [Seldner & Peebles 1977; see, however, Efstathiou 1988 (also Section 3.2.4)] is consistent with the cluster correlations and the trend observed above (Figure 8). Recent observations of clusters of different types and richnesses (see summary

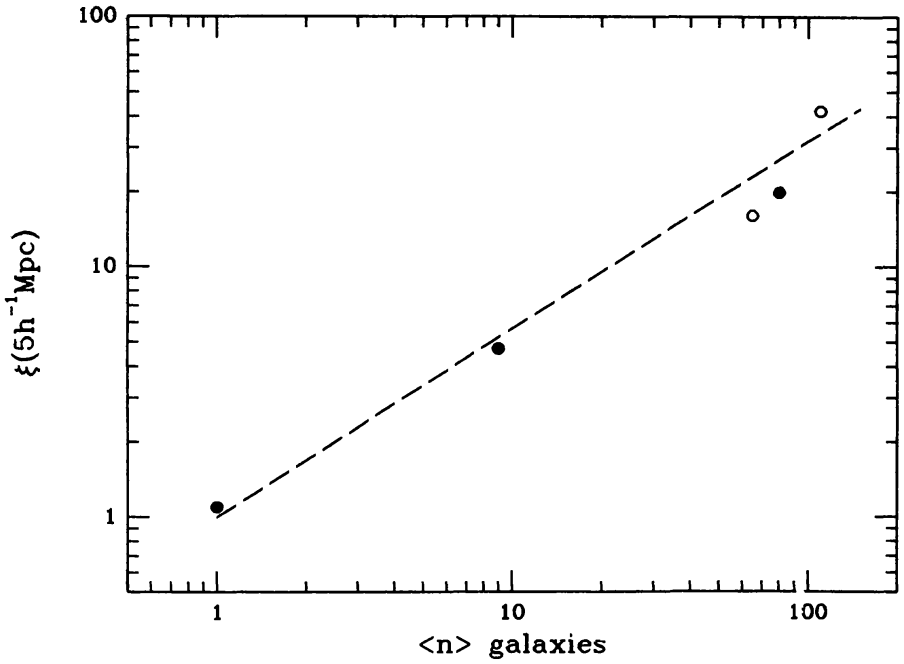

Figure 8 The dependence on richness of the two-point spatial correlation function suggested by BS83. The spatial correlation function at $r = 5h^{-1}$ Mpc is plotted as a function of richness for the galaxy-galaxy, galaxy-cluster, and cluster-cluster pairs ($R \geq 1$, as well as $R = 1$ and $R \geq 2$ independently; the latter two are shown by open circles). The dashed line, $\xi(n) \propto n^{0.8}$, is presented in order to guide the eye in the approximate richness dependence of the correlation (Sections 3.2, 3.5).

below) yield results that are consistent with the richness trend suggested by BS83 (Section 3.5).

Klypin & Kopylov (1983) investigated the spatial correlation function of a nearby sample of Abell clusters similar to the one described above, supplementing available redshift data with their own observations. Their sample includes 158 Abell clusters of all richness classes [$R \geq 0$ (i.e. including the somewhat incomplete class of $R = 0$ clusters] in distance group $D \leq 4$ and located at $|b| \geq 30°$. Their results are consistent with those of BS83. They find $\xi_{cc}(r) = (r/25)^{-1.6}$ for their observed range of $r \lesssim 50h^{-1}$ Mpc. The approximately 10% difference in slope is within the 1σ uncertainty of the slope determination estimated by BS83 (10%).

The earlier work of Hauser & Peebles (1973) used power-spectrum analysis and angular correlations to investigate the distribution of clusters in the Abell catalog. They also find evidence for strong superclustering of clusters and show that the degree and angular scale of the apparent superclustering varies with distance in the manner expected if the clustering is intrinsic to the spatial distribution rather than a consequence of patchy local obscuration.

Additional investigations of the spatial distribution of rich clusters of galaxies in the Abell catalog include those by Kalinkov et al. (1985), Batuski & Burns (1985a), Postman et al. (1986), Shvartsman (1988), and Szalay et al. (1988). These studies investigate different subsamples of the catalog, to different distances, regions, and/or richnesses, as well as apply different techniques and/or corrections. All the investigations yield consistent results with those described above, as summarized below.

Kalinkov et al. (1985) find a spatial correlation function for rich ($R \geq 1$) Abell clusters, using new redshift estimator calibrations and richness corrections, of $\xi_{cc}(r) = (r/22.4)^{-1.9}$ for $r \lesssim 80h^{-1}$ Mpc.

Batuski & Burns (1985a) determined the spatial correlation function for Abell clusters of all richness groups ($R \geq 0$) to $z \simeq 0.085$. Their sample includes 226 clusters. (The higher spatial density of this sample as compared with the $R \geq 1$ sample is due to the inclusion of the $R = 0$ clusters.) For this sample they find $\xi_{cc}^{R \geq 0}(r) = 65r^{-1.5}$ for $r \lesssim 150h^{-1}$ Mpc. The somewhat shallower slope, while within 2σ of the 1.8 slope, may be partially due to the use of some estimated rather than measured redshifts, which reduces the correlations on small scales and flattens the slope (see BS83). When approximated as a -1.8 power-law slope, the function is $\xi_{cc}^{R \geq 0}(r) \simeq 200r^{-1.8} \simeq (r/19)^{-1.8}$. This correlation function is one order of magnitude stronger than the galaxy correlations and about 50% lower than BS83 correlation function for $R \geq 1$ clusters. The somewhat reduced correlation strength is consistent with the richness dependence suggested by BS83 and Bahcall & Burgett (1986) (Section 3.5).

Postman et al. (1986) reanalyzed the $D \leq 4$ sample used by Bahcall & Soneira, as well as a sample of 152 Abell clusters to $z \leq 0.1$. Their results are consistent with the BS83 correlation functions.

Shvartsman (1988) and Kopylov et al. (1987) used the 6-m USSR telescope to measure redshifts of all very rich ($R \geq 2$) Abell clusters to $z \lesssim 0.23$, located at $b > 60°$. They calculated the spatial correlation function of this deep sample of very rich clusters, which includes 50 clusters in the redshift range $0.10 \leq z \leq 0.23$. They find $\xi_{cc}^{R \geq 2}(r) = (r/40)^{-1.5 \pm 0.5}$ for the range $5 \lesssim r \lesssim 50h^{-1}$ Mpc, consistent with the BS83 correlations of very rich ($R \geq 2$) clusters and with the suggested increase of correlation strength (and length) with richness. The correlation scale for the $R \geq 2$ clusters is $\sim 40h^{-1}$ Mpc, while the correlation scale for the $R \geq 1$ clusters is $\sim 25h^{-1}$ Mpc. The above authors also report weak but positive correlations at much larger separations: $\xi(100\text{–}150h^{-1}\ \text{Mpc}) = 0.47 \pm 0.14$. A similar result is suggested by Batuski et al. (1988). This is comparable to the supercluster correlation results of Bahcall & Burgett (1986) (Section 3.4), who detect similar marginal (3σ) correlations. Systematic effects, however, which may be important on these scales, are difficult to assess.

Huchra (1988) used a deep redshift sample ($z \lesssim 0.2$) of Abell clusters complete over a small region of the northern sky. He finds $\xi_{cc}(r) \sim (r/20)^{-1/8}$ for $R \geq 0$ clusters, consistent with the results discussed above.

The new Southern Hemisphere catalog of rich clusters (Abell et al. 1988; see Section 2) can also be analyzed for structure. Bahcall et al. (1988b) have recently analyzed the distribution of clusters in this catalog. The results suggest that the correlation function of clusters in the southern sky is consistent with the results presented above for northern clusters.

3.2.2 SHECTMAN CLUSTERS Shectman (1985) used the Shane-Wirtanen counts to identify clusters of galaxies by finding local density maxima above a threshold value, after slightly smoothing the data to reduce the effect of the sampling grid. A total of 646 clusters of galaxies were identified using the specified selection algorithm (Section 2).

The radial velocity distribution of these clusters is similar to the radial velocity distribution of Abell clusters of distance class $D \leq 4$ as determined by Shectman from comparisons of velocity data for a complete sample of 112 clusters. The space density of the Shectman clusters is therefore ~ 6 times greater than the space density of the 104 $R \geq 1$, $D \leq 4$ Abell cluster sample.

The angular two-point correlation function of the Shectman clusters at $|b| \geq 50°$ (a sample of 488 clusters in total) was determined by Shectman (1985). The implied spatial correlation function is $\xi_{cc}(r) \simeq 180r^{-1.8} \simeq$

$(r/18)^{-1.8}$. This correlation function is about 10 times larger than the galaxy correlation (Equation 5) and is about a factor of 2 lower than the rich ($R \geq 1$) cluster correlations (Equation 4). Since the space density of the Shectman clusters is ~ 6 times higher than the density of the $R \geq 1$ clusters, and thus the identifications of the former are with poorer clusters, the results of the Shectman cluster correlations are consistent both with those of the Abell clusters and with the trend suggested by Bahcall & Soneira of increased correlation strength with cluster richness (Section 3.5). Recently, S. Shectman (private communication, 1988) determined the redshifts of all clusters in the sample, enabling the direct determination of the cluster spatial correlation function. The spatial function was observed to be in agreement with the implied spatial correlation function discussed above.

3.2.3 ZWICKY CLUSTERS The angular distribution of clusters in the Zwicky (1961–1968) catalog was analyzed by Postman et al. (1986). The cluster selection algorithm in the Zwicky catalog differs markedly from the cluster selection definition of Abell (Section 2). Abell's definition of a cluster relates to the cluster intrinsic properties (i.e. the number of galaxies within a given *linear* scale and a given *absolute* magnitude range) and thus is independent of redshift (except for standard selection biases). Zwicky's clusters are defined relative to the mean density of the field, with varying cluster sizes and contours, and all galaxies down to the plate limit are considered. Therefore, the cluster selection is by definition strongly dependent on redshift. A direct comparison between the correlation functions of Zwicky and Abell clusters is therefore not straightforward. However, an uncorrected comparison will test to some extent the universality of the cluster correlation function, with its suggested dependence on richness, as well as further test the sensitivity of the correlation function to the cluster identification procedure.

It is found that in the distance range where Abell and Zwicky identify clusters of comparable overdensity (1173 Distant Zwicky clusters with $z \simeq 0.1$–0.14), the correlation functions of the Abell and Zwicky clusters are indeed the same in the scale range studied ($r \lesssim 60h^{-1}$ Mpc). The angular correlation functions of the two nearer samples of the Zwicky clusters (377 Near clusters and 680 Medium-Distant clusters) are observed to be weaker (when scaled to the same depth as the $D \leq 4$ Abell sample) than the rich ($R \geq 1$) Abell clusters. Since these nearer Zwicky clusters are by definition much poorer clusters, with a considerably higher space density than the $R \geq 1$ Abell clusters, they are expected to have a weaker correlation strength (BS83; see also Section 3.5).

A comparison of the cluster correlation functions determined by the

various investigators discussed above using different catalogs and samples is summarized in Figures 9*a* and 9*b*. *A general agreement is observed among all the results. The consistency of the correlation functions determined from different catalogs, cluster selection criteria, redshift and richness ranges, and by different investigators strongly supports the reality and universality of the cluster correlations described in this section.*

3.2.4 GALAXY-CLUSTER CROSS-CORRELATIONS The angular cross-correlation between the galaxy distribution in the Shane-Wirtanen galaxy counts and the positions of rich Abell clusters was studied by Seldner & Peebles (1977) and more recently by Efstathiou (1988). This cross-correlation function, $w_{gc}(\theta)$, measures the excess probability, over random, of finding a galaxy within a given separation from a cluster (i.e. it describes the enhanced density of galaxies around a cluster).

Seldner & Peebles (1977) find that the angular function $w_{gc}(\theta)$ scales with cluster distance-class D as expected from the galaxy luminosity function. The $w_{gc}(\theta)$ estimates are reasonably well fitted by a two-power-law model for the spatial function $\xi_{gc}(r)$ (Peebles 1980b):

$$\xi_{gc}(r) = (r/7)^{-2.5} + (r/12.5)^{-1.7}, \qquad r \lesssim 40h^{-1}\ \text{Mpc}. \tag{12.}$$

The enhancement of Lick counts around cluster centers is traced to $r \sim 40h^{-1}$ Mpc before it is lost in the noise.

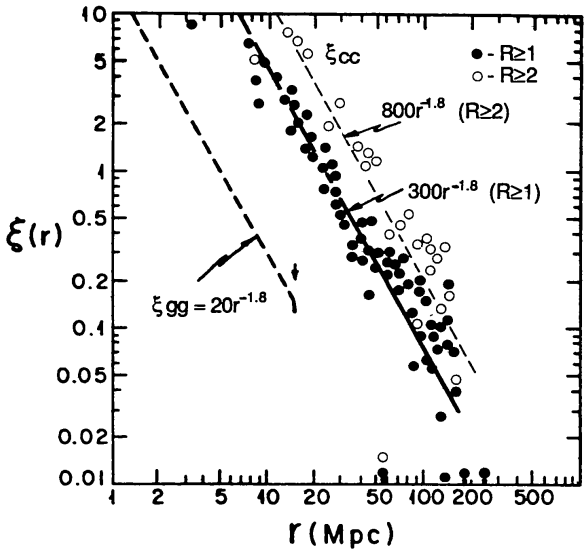

Figure 9a A composite of the spatial cluster correlation function determined by different investigators from different cluster samples [Abell clusters to different depths ($z \simeq 0.08$ through $z \simeq 0.24$), different richnesses, and different regions; see Section 3). The BS83 correlation function, $300r^{-1.8}$, is shown (see Figure 3); the results of the different samples are all consistent with this function. The richer $R \geq 2$ clusters exhibit stronger correlations, as suggested by BS83 (Sections 3.2, 3.5).

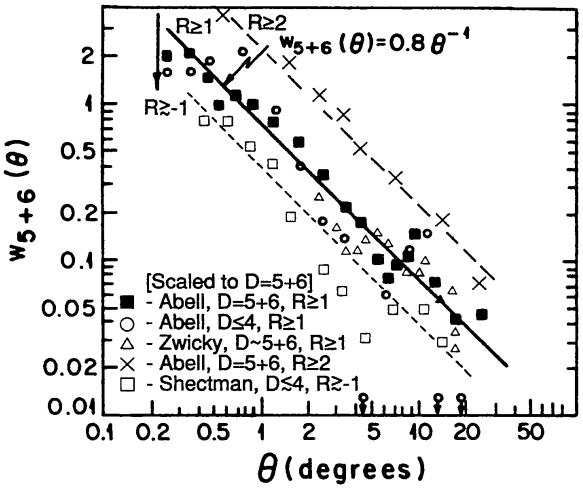

Figure 9b A composite of the angular cluster correlation function determined from different catalogs and samples (indicated by the different symbols; see Section 3). All results are scaled to the $D = 5+6$ distance. The BS83 correlation function for the $D = 5+6$ clusters (Figure 4) is indicated by the solid line. The consistency among the different samples, as well as the dependence of the correlation strength on richness (Sections 3.2, 3.5), are apparent.

The first term of the galaxy-cluster cross-correlation (Equation 12) represents the "standard" internal density profile of galaxies in a cluster (which generally has the shape of a bounded isothermal sphere; e.g. Bahcall 1977). The more slowly varying part of the cross-correlation function found at larger scales and represented by the $r^{-1.7}$ part of Equation 12 is produced by the clustering of clusters, as discussed in the previous subsections (i.e. galaxies from one cluster provide excess concentration of galaxies near a neighboring "correlated" cluster). The above cross-correlation is consistent with the cluster-cluster correlation function discussed in Section 3.2.1 (Equation 4). It is expected that the cross-correlation term will be a geometrical mean of the correlation functions of the galaxies and clusters. Thus, it is expected that

$$\xi_{gc}(r) \simeq \xi_{gg}^{1/2}(r)\xi_{cc}^{1/2}(r). \qquad 13.$$

Using the galaxy and cluster correlation functions discussed in Section 3.2.1, i.e. $\xi_{gg} \simeq 20r^{-1.8}$ and $\xi_{cc} \simeq 360r^{-1.8}$, the expected cross-correlation term is $\xi_{gc} \simeq 85r^{-1.8}$. This compares remarkably well with the second term of Equation 12, $\xi_{gc}(r/12.5)^{-1.7} \simeq 73r^{-1.7}$. This result implies that the cluster correlation function is stronger by a factor of about 16 than the galaxy correlations, and that it extends to scales of at least $40h^{-1}$ Mpc, as is observed directly.

Recently, however, Efstathiou (1988) re-analyzed the galaxy-cluster cross-correlations using only the subsample of clusters for which redshift measurements are available, finding a somewhat weaker and less extended

galaxy-cluster cross-correlation function. A more complete redshift sample of clusters may be needed before a galaxy-cluster cross-correlation function can be established with greater precision.

3.3 *Supporting Evidence for the Cluster Correlation Function*

I summarize below several observations that support the physical reality of the cluster correlation function discussed above.

1. The angular cluster correlation function scales with depth as expected from spatial correlations, rather than from patchy obscuration or systematic omission (Hauser & Peebles 1973, BS83).
2. The projected and redshift cluster correlation functions yield consistent results, thus indicating the physical reality of the correlations.
3. The cluster correlation function yields consistent results in different large regions of the sky (e.g. north vs. south, high vs. low latitudes, different longitude ranges; see BS83). The estimated scatter, or uncertainty, in the correlation function is approximately $\pm 15\%$ in the correlation scale (i.e. approximately $\pm 25\%$ in the amplitude).
4. The cluster correlations determined from the Abell sample are consistent with more recent results using other samples and catalogs [e.g. Shectman clusters (Shectman 1985), Zwicky clusters (Postman et al. 1986), southern Abell et al. (1988) clusters (Bahcall et al. 1988b), and subsamples of different regions, redshifts, and richnesses in the Abell catalog (BS83, Batuski & Burns 1985a, Postman et al. 1986, Shvartsman 1988, Szalay et al. 1988); see Figure 9]. These comparisons provide a strong test of the sensitivity of the correlation function to the cluster identification procedure. The scatter in the correlation scale-length is $\sim \pm 15\%$; the average scale length is $r_0 = 23 \pm 3h^{-1}$ Mpc for $R \geq 1$ clusters.
5. The cluster correlation function is consistent with the galaxy-cluster cross-correlation function determined by Seldner & Peebles (1977). It is less consistent, however, with the cross-correlation results of Efstathiou (1988).
6. A preliminary estimate of the completeness limit of the nearby Abell sample obtained by comparisons with X-ray data of galaxy clusters yields a reasonably high completeness level for the sample (work in progress by N. A. Bahcall, T. Maccacaro, I. M. Gioia et al.). Of the 25 nearest clusters in the sample, all but one are detected as extended X-ray sources with luminosities appropriate to rich clusters. (The twenty-fifth cluster has an upper limit consistent with the expected luminosity.) In addition, preliminary results of the Einstein Medium Deep X-Ray

Survey show that no extended X-ray cluster is found that should have been a rich cluster in Abell's nearby sample but was missed (out of approximately four real clusters expected within the survey area, i.e. completeness of better than $\sim 75\%$).

The evidence listed above supports the reality of the cluster correlation function and suggests that it is unlikely that the correlations are mainly a result of catalog biases or omissions. A determination of the cluster correlation function from catalogs with automated selection procedures will improve the accuracy of the intrinsic cluster correlations, especially at large separations where the correlations are rather weak.

3.4 *Supercluster Correlations*

Bahcall & Burgett (1986) carried the study of rich galaxy clusters one step further by studying the spatial distribution of superclusters. The sample used was the Bahcall & Soneira (1984) complete catalog of superclusters to $z \leq 0.08$, where superclusters are defined as groups of rich clusters and identified by a spatial density enhancement of clusters. All volumes of space with a spatial density of clusters f times larger than the mean cluster density are identified in the above catalog as superclusters for a specified value of f (Section 6.1). The supercluster selection process was repeated for various overdensity values f, from $f = 10$ to $f = 400$, yielding specific supercluster catalogs for each f value. A total of 16 superclusters are cataloged for $R \geq 1$ and $f = 20$, and 26 superclusters for $R \geq 0$ and $f = 20$.

The spatial correlation among the superclusters was determined by Bahcall & Burgett (1986) for samples of different richness and overdensity. Because of the large size of the superclusters themselves, no meaningful correlations are expected at small separations ($\lesssim 50h^{-1}$ Mpc). In addition, no detectable correlations are expected at very large separations ($> 200h^{-1}$ Mpc), since this scale is comparable to the limits of the sample. Any observable correlations are therefore expected only in a separation "window" around $\sim 100h^{-1}$ Mpc.

The results, presented in Figure 10, reveal correlations among superclusters on a very large scale: ~ 100–$150h^{-1}$ Mpc. Because of the small size of the supercluster sample, the statistical uncertainty is appreciable; the observed effect is at the 3σ level (as determined by comparisons with numerical simulations of random catalogs). In addition, all the samples with different overdensities and cluster richnesses show a similar effect at a similar scale length. The results imply the existence of very large-scale structures with scales of ~ 100–$150h^{-1}$ Mpc.

Similar results have been recently obtained by Kopylov et al. (1987) by studying correlations of very rich clusters to $z \lesssim 0.2$ (Section 3.2.1). They

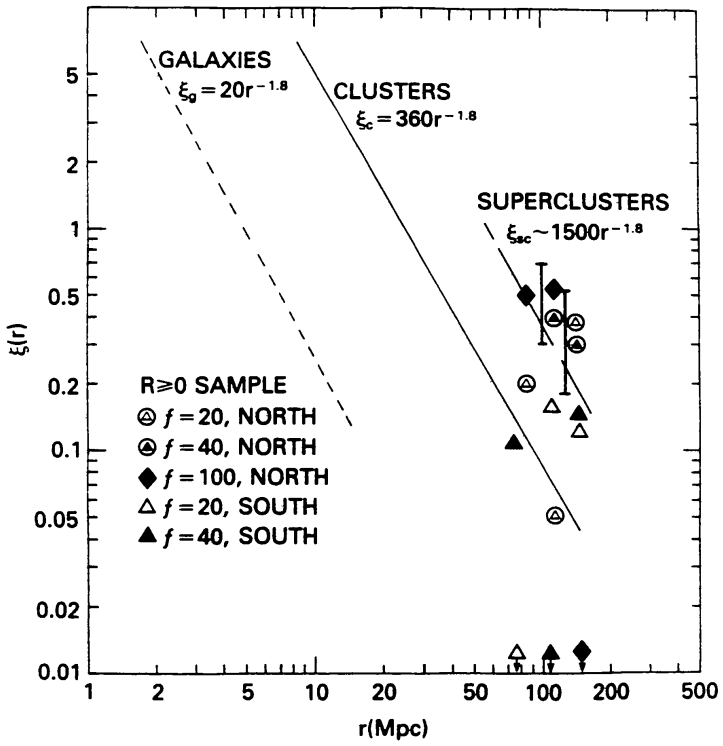

Figure 10 The spatial correlation of superclusters for the $R \geq 0$ sample (Bahcall & Burgett 1986). Different subsamples are indicated by different symbols. No meaningful correlations are expected below $\sim 50h^{-1}$ Mpc.

report $\xi_{cc}(100\text{–}150h^{-1}\ \text{Mpc}) = 0.47 \pm 0.14$. Tully's (1986, 1987b) observations of very large-scale structures in the cluster distribution, up to $\sim 300h^{-1}$ Mpc, may also reflect the above observed tendency of superclusters to cluster.

Figure 10 shows that the supercluster correlation strength is stronger than that of the rich-cluster correlations by a factor of approximately 4. It is approximately two orders of magnitude stronger than the galaxy correlation amplitude. While this enhancement is observed in the $\sim 100\text{–}150h^{-1}$ Mpc range, it is possible that the supercluster correlation function also follows an $r^{-1.8}$ law. *If* the correlations follow an $r^{-1.8}$ law, then the function would satisfy the relation

$$\xi_{sc,sc}(r) \simeq 1500r^{-1.8} \simeq (r/60)^{-1.8}. \qquad 14.$$

The implied correlation scale of superclusters would be $60h^{-1}$ Mpc, as compared with $5h^{-1}$ Mpc for the correlation scale of galaxies (Groth & Peebles 1977) and $25h^{-1}$ Mpc for rich ($R \geq 1$) clusters (BS83). This apparent increase in correlation strength is consistent with the earlier prediction of BS83 of increased correlations with richness (luminosity) of the system.

The supercluster correlation amplitude fits well the predicted trend (Section 3.5).

3.5 *Richness Dependence of the Correlation Function*

As discussed above, the cluster correlation function appears to depend strongly on cluster richness (BS83), with richer clusters showing stronger correlations than poorer clusters. This result, combined with the lower correlation amplitude of individual galaxies, led Bahcall & Soneira to the conclusion that progressively stronger correlations exist, at a given separation, for richer or more luminous galaxy systems (Figure 8, Section 3.2.1). Several recent studies of the correlations of other types and richnesses of clusters, reviewed above [Batuski & Burns (1985a), Shectman (1985), and Postman et al. (1986) for poorer clusters; Kopylov et al. (1987) for richer clusters; Bahcall & Burgett (1986) for superclusters] appear to be consistent with the trend suggested by Bahcall & Soneira and later expanded by Bahcall & Burgett (1986). This dependence of correlation strength on richness is summarized in Figure 11. It can be approximated roughly as follows:

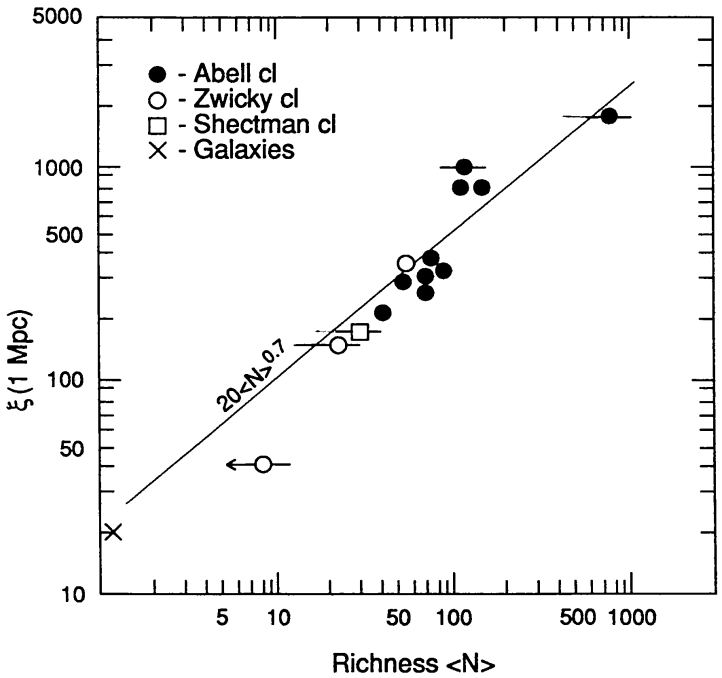

Figure 11 The dependence of the correlation function strength on the mean richness ($\propto$luminosity) of the system (Bahcall & Burgett 1986). The results are for clusters from different catalogs (Abell, Zwicky, and Shectman, as indicated by the symbols), determined by different investigators for samples of different richnesses, depths, and regions (Section 3). The correlation strengths for galaxies and superclusters are also included. The solid line indicates the approximate dependence on richness [compare, e.g., with the BS83 original dependence (Figure 8)].

$$\xi(1\ \text{Mpc}) \sim 20N^{0.7} \sim 20(L/L^*)^{0.7} \sim 20(M/10^{12}M_\odot)^{0.5}, \quad 15.$$

where N is the richness of the system [for galaxies, $N = 1$; for clusters, N = Abell's richness definition (Section 2)], L is the luminosity (relative to L^* in the Schechter luminosity function), and M is the mass of the system. This relation suggests an *average trend* in the data and should not be regarded as an exact formula. (Obviously, the relation between N, L, and M is not unique; for a given N, different L's and M's may apply, and vice versa. The difference between the M versus the L slope is due to the higher observed M/L ratios for clusters than for galaxies).

The correlation-richness dependence suggests that rich clusters populate the large-scale structures, or superclusters, more abundantly than galaxies do relative to their mean space densities. It also implies that rich clusters are indeed an efficient tracer of large-scale structure in the Universe.

A continuous richness dependence of the correlation strength indicates that no unique correlation function exists for all luminous systems (see, however, Section 4 for a possible universal *dimensionless* correlation function). It therefore places a new emphasis on the question of what is the underlying mass correlation function in the Universe: Which "richness" or "luminosity" equivalent in Figure 11 does the mass follow? And, specifically, should it follow, as usually assumed, the correlation function of galaxies? (The latter may itself be a continuous function of the luminosity or some other property of galaxies.) Could the mass-correlation amplitude correspond to an extrapolation of Figure 11 (or relation 15) to objects with an even lower richness (or luminosity or mass) than galaxies, and thus with weaker clustering properties than galaxies? This question led to the idea of biased galaxy formation models (e.g. Kaiser 1984, Bardeen et al. 1986), where the mass distribution is assumed to be considerably less clumped than galaxies, and galaxies form in a "biased" way only at higher density peaks of the mass distribution. In this picture, a large fraction of the dark matter in the Universe is not attached to luminous galaxies but rather is floating as smaller dark clouds, more smoothly distributed in space.

Several explanations of the observed increase of correlation with richness have been suggested, although the phenomenon is still not fully understood. Kaiser (1984) suggested applying the statistics of rare events. If the density perturbations are described by a random Gaussian field, and if the regions where clusters form correspond to densities higher than a given threshold, then the correlation function of the points above the

threshold is amplified over the correlation function of the underlying point distribution. By filtering out scales smaller than clusters from the initial power spectrum and selecting the appropriate threshold, it is possible to match the enhanced correlations of the Abell clusters if the latter correspond to $\geq 3\sigma$ fluctuations (see, however, Coles 1986). The model may have difficulty, however, in explaining the positive cluster correlations observed at $r \gtrsim 20h^{-1}$ Mpc, where the galaxy correlations are negative or zero.

Several galaxy formation models, such as biased cold dark matter, hybrid scenarios, and cosmic strings, can reproduce a trend of increasing correlation strength from galaxies to clusters; these are discussed in Section 9.

4. A UNIVERSAL CORRELATION FUNCTION

The increase of correlation strength with richness implies that rich, luminous systems are more strongly clustered, at a given separation, than poorer systems. The power law of the correlation functions is also observed to be identical in the various systems studied. Either initial conditions, or subsequent evolution, may be responsible for the observed phenomena. Since the observed correlation functions follow the same power law ($r^{-1.8}$), the effect of increased correlation strength with richness (at a given separation) can also be expressed as a scale shift in the correlation functions (Szalay & Schramm 1985). In Figure 12 I plot the amplitude of the correlation functions of the various systems (galaxies, poor and rich clusters, superclusters) as a function of the mean separation of objects in the sample, d (see Bahcall & Burgett 1986, Bahcall 1987). The mean separation is related to the mean spatial density of objects in the sample, n, through $d = n^{-1/3}$. For example, the mean separation of galaxies is about 5 Mpc, while the mean separations of $R \geq 1$ and $R \geq 2$ clusters are, respectively, about 50 Mpc and 70 Mpc.

It is apparent from Figure 12 that the correlation strength increases with the sample's mean separation. Moreover, a dimensionless correlation function normalized to the sample's mean separation d appears to yield a constant, universal function for nearly all the systems studied (some enhancement is required for galaxies, as described below). This universal dimensionless correlation function has the form

$$\xi_i(r) \simeq 0.3(r/d_i)^{-1.8} \simeq (r/0.5d_i)^{-1.8}, \qquad 16.$$

where the index i refers to the system being considered, and d_i is its mean separation. Relation 16 implies a universal dimensionless correlation amplitude of ~ 0.3, and, equivalently, a universal correlation scale of

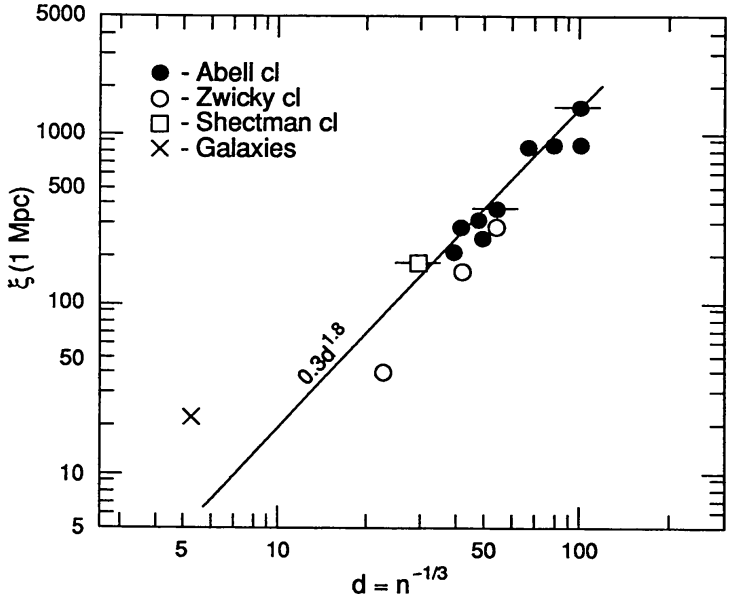

Figure 12 The dependence of the correlation function on the mean separation of objects in the system. The results are for clusters from different catalogs (Abell, Zwicky, and Shectman, as indicated by the symbols), determined by different investigators for samples of different mean densities (i.e. mean separations) (Section 3). The correlation strengths for galaxies and superclusters are also included. The solid line represents a $d^{1.8}$ dependence (e.g. Szalay & Schramm 1985, Bahcall & Burgett 1986).

$r_0 \simeq 0.5 d_i$. The correlation function of galaxies is stronger than that expressed by relation (16) by a factor of about four (Figure 12). The universality of the correlation function suggests a scale-invariant clustering process (Szalay & Schramm 1985). The stronger dimensionless galaxy correlations may imply gravitational enhancement on smaller scales. If a nonlinear process, other than gravity, participates in galaxy formation, and this process is scale-invariant, the created structure will have a single power-law correlation function, the slope of which (α) is related to the geometry of the structure (i.e. its fractal dimension β). The latter is related to the correlation function slope via $\alpha = \beta - 3$ (see, e.g. Mandelbrot 1982). The fractal dimension of the universal structure implied by the above data is therefore $\beta \simeq 1.2$. Small-scale gravitational clustering may break the scale invariance and increase the dimensionless correlation amplitude for galaxies.

We do not know yet what physical process can create a scale-invariant structure with $\beta \simeq 1.2$. An innovative suggestion involves cosmic strings as the primary agent in the formation of galaxies and clusters; this model appears to create such a scale-invariant infrastructure (Turok 1985). The model yields a scale-invariant correlation function similar to that observed, with a power law of -2 (as implied by one-dimensional "string" structures

with fractal dimension of unity). More detailed calculations with cosmic string models are currently being carried out by several investigators (Section 9).

5. PHENOMENOLOGICAL CLUSTERING MODELS

5.1 *Long Tails to Galaxy Clusters*

The galaxy correlations depend, at least partially, on the rich cluster correlations, since clusters contain galaxies. If all galaxies were members of rich clusters, the two correlation functions should be approximately the same on large scales. The fraction of galaxies in clusters is clearly less than unity. The fraction of galaxies, f, that are associated with rich clusters represents the probability that a randomly chosen galaxy is correlated with a rich cluster. These associations may include large structures (tens of megaparsecs), comparable to the separations observed in the cluster correlation function (and well above the standard Abell radius of $1.5h^{-1}$ Mpc).

The galaxy correlation function contains contributions from three terms (Bahcall 1986): galaxy pairs from the fraction f of galaxies that are cluster members, pairs from the fraction $1-f$ of galaxies that are noncluster members ("field"), and cross-term pairs. Inserting the analytic expressions for each of these terms into the expression for the overall galaxy correlation function yields

$$\left(\frac{\xi_{cc}}{\xi_{gg}}\right)^{1/2} = \frac{1-(1-f)\,(\xi_{gg}^{f}/\xi_{gg})^{1/2}}{f}. \qquad 17.$$

The above ratio of the cluster to galaxy correlation strength depends on two parameters: the fraction of galaxies in clusters, f, and the ratio of the "field" galaxy correlation strength, ξ_{gg}^{f} (i.e. the correlation of the $1-f$ fraction of galaxies outside the rich clusters) to the overall galaxy correlation ξ_{gg}. If all galaxies were associated with rich clusters, i.e. $f = 1$, then the galaxy and cluster correlations are identical on large scales, as expected. However, for any fraction $f < 1$, the galaxy correlations will be smaller than the parent cluster correlations due to the reducing effect of the less clustered "field" galaxies. Figure 13 represents graphically Equation 17. The curves are the expected $\xi_{cc}/\xi_{gg}(f)$ relations for selected values of the parameter $x \equiv \xi_{gg}^{f}/\xi_{gg}$. The observed correlation strengths are represented by the data points. The observed ratio $\xi_{cc}/\xi_{gg} \simeq 18$ for $R \geq 1$ clusters yields a fraction of galaxies in clusters that ranges from $f \simeq 25\%$ for $x \simeq 0$ to $f \simeq 15\%$ for $x \simeq 1/4$. Therefore, if approximately 20% of all galaxies are

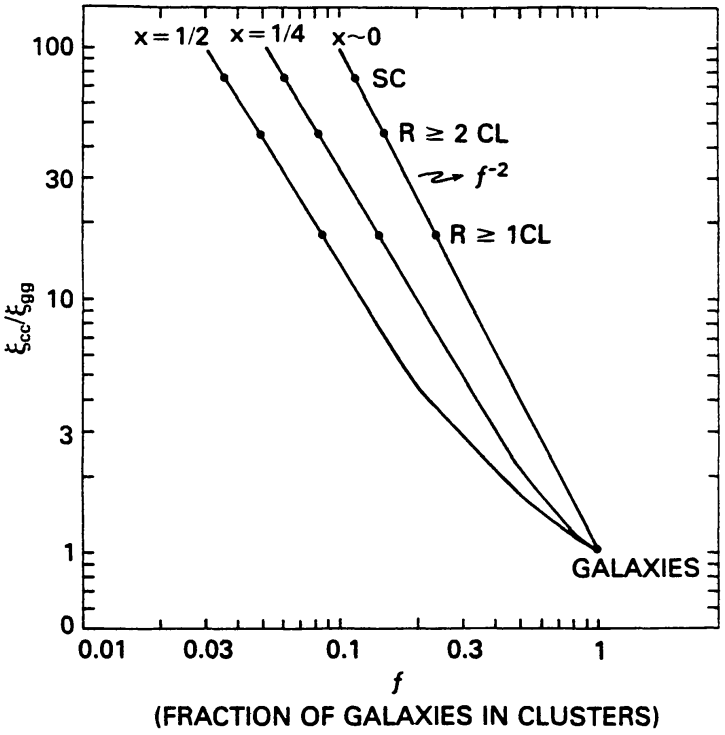

Figure 13 The ratio of the cluster to galaxy correlation functions predicted from Bahcall's (1986) model (Equation 17) is plotted as a function of the fraction f of galaxies associated with the clusters. The different curves represent different values of the "field" (noncluster) correlation strength, ξ^f_{gg}, in terms of the ratio parameter $x = \xi^f_{gg}/\xi_{gg}$. The observed correlation strengths of $R \geq 1$ clusters, $R \geq 2$ clusters, and superclusters are indicated by the points.

associated with rich ($R \geq 1$) clusters, the galaxy correlation function will be, as observed, ~ 18 times weaker than the cluster correlations.

The model suggests (Bahcall 1986) that the fraction of galaxies associated with rich clusters is considerably larger than previously believed; most of these galaxies would be distributed in the outer tails of the clusters, which may extend to at least $\sim 30h^{-1}$ Mpc. Most clusters are therefore predicted to be embedded within much larger structures. Possible physical models that can create such extended structures, with clusters forming in preferentially high-density regions and galaxies forming at lower density regions, are briefly discussed in Section 9.

The model makes testable predictions that can be studied with complete redshift surveys. Recent redshift surveys of galaxies (Section 7) indeed suggest that clusters are generally embedded in large elongated structures that contain a considerable fraction of galaxies. This picture is qualitatively consistent with the phenomenological model described above.

The long-tail model may also explain the negligible correlations observed among Lα clouds in quasi-stellar object (QSO) spectra (Sargent

et al. 1980). If the clouds can only exist in the field (noncluster environment) because clusters have too large an ambient pressure, then they would not be expected to have significant correlations.

5.2 *The Shell Model*

Galaxies may be distributed on surfaces of shells (or cells), with rich clusters located at shell intersections. This picture is suggested by redshift surveys of galaxies (Gregory et al. 1981, Giovanelli et al. 1986, de Lapparent et al. 1986). In order to test this "shell" model and its agreement with the observed galaxy and cluster correlations, Bahcall et al. (1988a) made simulations in which they placed galaxies on surfaces of randomly distributed shells and formed clusters at the shell intersections (see also Bahcall 1988a). They found that the model cluster correlations are consistent with the observed cluster correlations, including the large increase in correlation strength from galaxies to clusters. The results are not very sensitive to the exact parameters used. The model galaxy correlations appear to be consistent with observations on small scales, but they exhibit a tail of weak positive correlations at larger separations that are not seen in the data.

An example of results from a typical model is shown in Figure 14; more details are given in Bahcall et al. (1988a). The results suggest that the observed cluster correlations may be simply due to the geometry of clusters positioned on randomly placed shells or similar structures; the typical structure size is best fit with a radius of approximately $20h^{-1}$ Mpc. Similar simulations based on the explosion model for the formation of shells were recently performed by Weinberg et al. (1988). They too find a strong increase in correlation strength from the galaxy to the cluster correlation function.

6. SUPERCLUSTERS AND VOIDS

In this section I consider the superclustering of clusters and discuss the identification and properties of individual superclusters. This approach complements the statistical studies of correlation functions, providing specific information about type, shape, structure, and content of superclusters. For a recent review paper on *superclusters*, see Oort (1983). A review of *voids* is presented in this volume by Rood (1988).

6.1 *Supercluster Catalogs*

In order to investigate the properties of the large-scale clustering of clusters, a complete, well-defined catalog of superclusters—defined as clusters of clusters of galaxies—is required. Early lists of superclusters

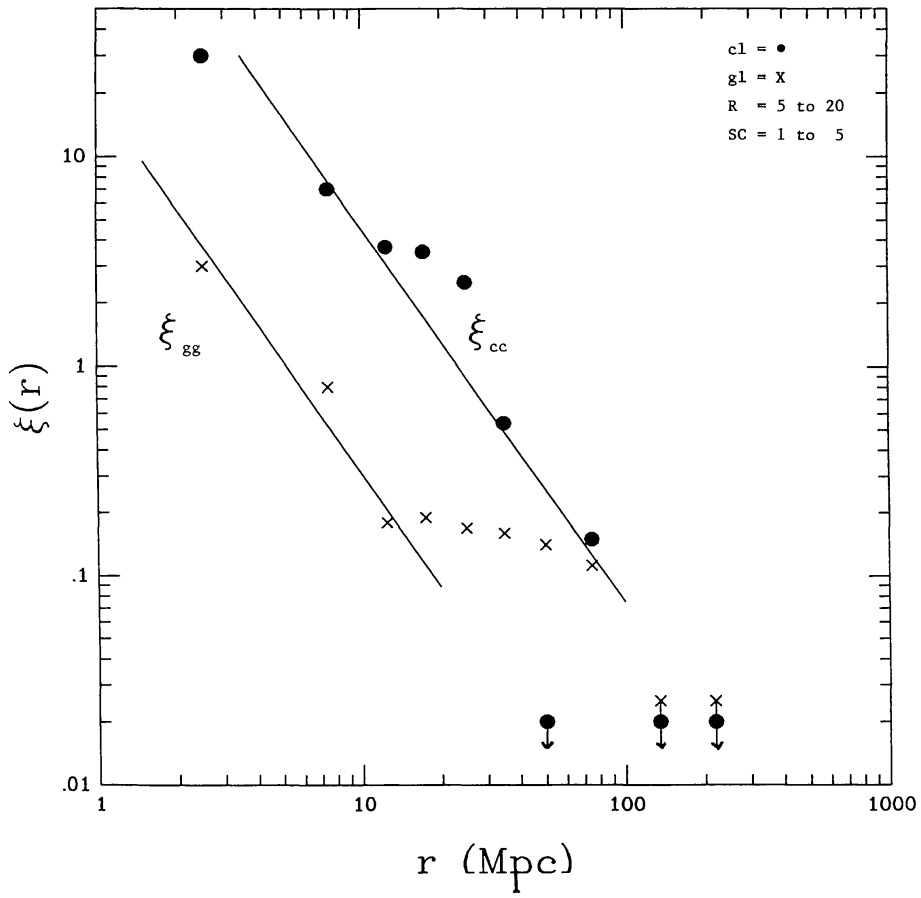

Figure 14 Shell-model correlation functions (Bahcall et al. 1988a) for clusters (dots) and galaxies (crosses), and their comparisons with observations (ξ_{gg} and ξ_{cc} lines). The plotted model represents a shell radius distribution in the range 5 to $20h^{-1}$ Mpc, and, depending on size, 1 to 5 clusters forming at shell intersections (Section 5.2).

(e.g. Abell 1961, Rood 1976, Murray et al. 1978) used the projected distribution of rich Abell clusters plus estimated cluster redshifts (from Abell's magnitudes of the tenth brightest cluster galaxy), since very few redshift data were available. (The latter were used by Rood 1976.) Later on, Thuan (1980) used measured redshifts of the 77 nearest Abell clusters, with a single selection parameter; no comparisons with random catalogs were available. More recently, Bahcall & Soneira (1984) (hereinafter BS84) constructed a supercluster catalog to $z \leq 0.08$ using the complete redshift sample of 104 nearby Abell clusters ($D \leq 4$, $z \lesssim 0.1$) described in Section 2 and an objective selection criterion of a spatial density enhancement. I describe below the main properties of these catalogs.

In the BS84 catalog, all volumes of space with a spatial density of clusters f times larger than the mean cluster density are identified as superclusters for a specified value of f. The superclusters densities are therefore given by

$$n(\mathrm{sc}) = f n_0, \qquad 18.$$

where n(sc) is the spatial density of clusters in the supercluster, and n_0 is the mean cluster density in the sample. The supercluster selection process was repeated for various overdensity values f, from $f = 10$ to $f = 400$, yielding specific supercluster catalogs for each f value. The higher overdensity values identify the dense cores of superclusters; lower f values represent superclusters with lower densities and include the outskirts of high-density superclusters. The supercluster boundaries clearly do not set strict physical limits on the superclusters but rather define volumes of various levels of overdensities. The procedure was carried out for the redshift sample of 104 clusters of richness $R \geq 1$, as well as for the larger redshift sample of 175 $R \geq 0$ clusters.

A map of the supercluster catalog for the $R \geq 0$ sample is presented in Figure 15. Additional supercluster maps (e.g. the $R \geq 1$ sample), as well as a listing of the supercluster catalog itself and its member clusters for each of several f values, are given in BS84. A total of 16 superclusters are cataloged for $R \geq 1$ and $f = 20$, and 26 superclusters for $R \geq 0$ and $f = 20$.

Some global properties of the Bahcall-Soneira superclusters are summarized in Table 2. The number of clusters per supercluster varies from 2 to 15 for the $f = 20$ superclusters and reduces to a value of 2 to 3 clusters per $f = 400$ supercluster. The average number of clusters per supercluster is approximately three. The superclusters contain a large fraction of all clusters; this fraction, F_{cl}(sc), is 54% at $f = 20$ and reduces to 16% at $f = 400$. Comparisons with random catalogs show that these fractions are considerably higher than those expected by chance (Figure 16). This indicates that most of the high overdensity superclusters are real physical systems of the largest scale yet observed. The linear size of the largest observed superclusters are $\gtrsim 100h^{-1}$ Mpc (at $f = 20$; e.g. the Corona Borealis supercluster at $\sim 15^{\mathrm{h}} + 30°$). Elongated structures are suggested in these cases. The fractional volume of space occupied by the superclusters is, however, very small; it is $\sim 3\%$ at $f = 20$ and decreases rapidly with increasing f.

Figure 15 Projected area map of the northern (*top*) and southern (*bottom*) clusters and superclusters in the $D \leq 4$, $R \geq 0$ Abell sample (BS84). Outer contour is $|b| = 30°$; inner contour is the completeness of the sample. The Galactic poles are at the respective centers of these polar maps. Longitude l is 0° at the west and increases clockwise. The density contours represent the three-dimensional density enhancement of the superclusters, from $f = 20$ to $f = 400$ (Section 6). The Corona Borealis supercluster is at $\sim 15^{\mathrm{h}} + 30°$; Hercules is at $\sim 16^{\mathrm{h}} + 15°$; Ursa Major is at $\sim 11.5^{\mathrm{h}} + 55°$. For a map of the $R \geq 1$ superclusters, see BS84.

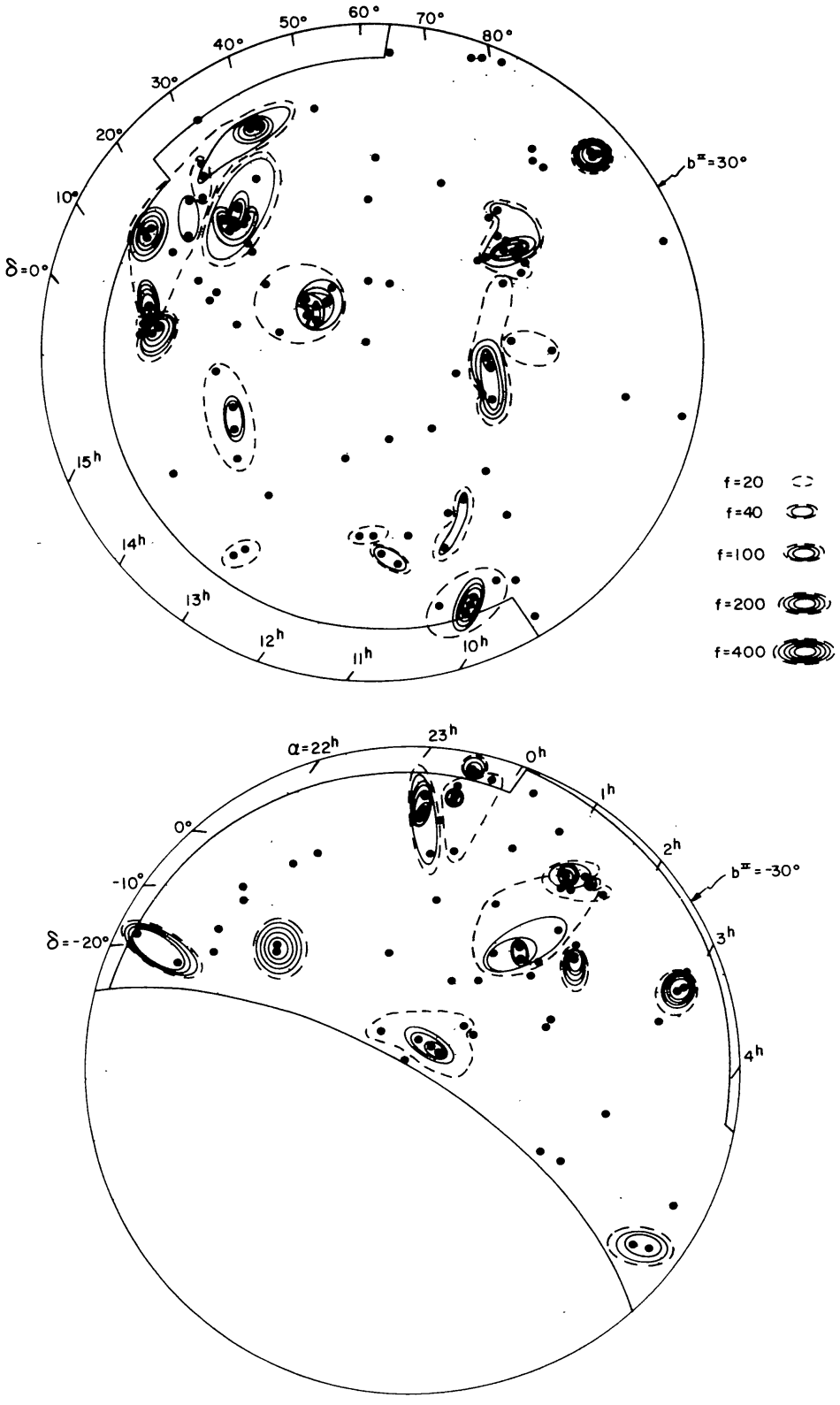

Table 2 Global properties of superclusters[a]

Property	f			
	20	40	100	400
N_{sc}	16	12	11	7
$n_{cl/sc}$	2–15	2–7	2–7	2–3
ΔR_{max} (Mpc)	145	36	36	13
$\langle \Delta R_x \rangle$ (Mpc)	27.1	7.6	7.6	4.5
$\langle \Delta R_z \rangle$ (Mpc)	28.6	14.5	13.5	4.5
F_{cl}(sc)	0.54	0.34	0.30	0.16
V_{sc}/V	0.03	0.008	0.003	0.0004

[a] The quantities listed are for the $R \geq 1$ sample. Notation: N_{sc}, total number of superclusters; $n_{cl/sc}$, number of $R \geq 1$ clusters per supercluster (i.e. supercluster richness); ΔR_{max}, linear size of the largest supercluster; $\langle \Delta R_x \rangle$ and $\langle \Delta R_z \rangle$, mean projected (one-dimensional) and redshift separations (in Mpc) of all cluster pairs in the superclusters; F_{cl}(sc), fraction of all $R \geq 1$ clusters that belong in superclusters; V_{sc}/V, fractional volume of space occupied by the superclusters.

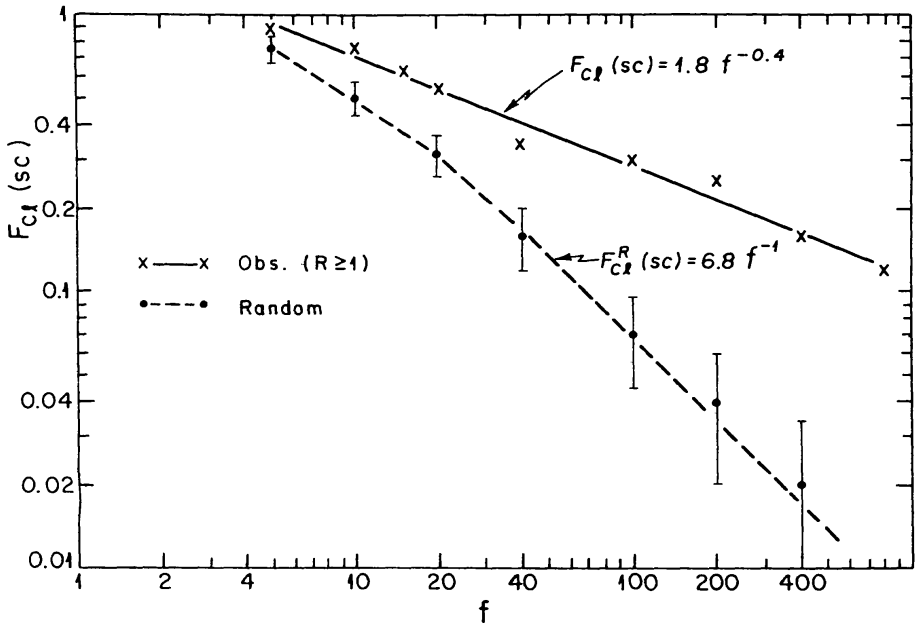

Figure 16 The fraction of all $R \geq 1$ clusters that are supercluster members as a function of the supercluster density enhancement f (BS84). Crosses represent the data; dots represent the ensemble average of 100 random catalogs. The 1σ error bars are shown for the random points. The curves are power-law fits for $f \gg 1$ (Section 6).

Thuan (1980) constructed a supercluster catalog from the nearest 77 Abell clusters by finding all cluster neighbors within a given separation of $65h^{-1}$ Mpc. While the selection criteria differ somewhat from those of BS84, there is general consistency between the catalogs.

Rood (1976) determined the superclustering of the nearest 27 Abell clusters using the clusters' measured redshifts and the criterion of having at least one cluster neighbor within $25h^{-1}$ Mpc. In the region of overlap, a general consistency exists among the Rood, Thuan, and Bahcall & Soneira catalogs. Kalinkov et al. (1984) determined the superclustering of the nearby Abell clusters using measured as well as estimated redshifts. Batuski & Burns (1985b) used measured as well as estimated redshifts (from Abell's m_{10} magnitude) for all Abell clusters in order to identify a large list of candidate superclusters. Further redshift measurements are required before the reality of these suggested superclusters can be determined.

6.2 *The Multiplicity Function of Superclusters*

Approximately one half of all rich clusters are observed to be members of superclusters (Section 6.1). The frequency distribution of clusters among superclusters of different richnesses, $n_{\mathrm{cl/sc}}$ (where $n_{\mathrm{cl/sc}}$ is the number of clusters in a supercluster), is the multiplicity function of the clusters, F_{cl} ($n_{\mathrm{cl/sc}}$). This multiplicity function was determined by BS84 for their complete sample of superclusters (Section 6.1) and compared with the multiplicity function expected from random samples.

The multiplicity function is presented in Figure 17, showing the fraction of clusters that are members of superclusters of any given richness. The frequency distributions are plotted for different values of density enhancement selection value f, from $f = 10$ to 400, for both the data and the average of 100 random cluster catalogs. Figure 17 shows that the observed and random catalogs yield different distributions. The fraction F_{cl} for the random catalog falls off smoothly and steeply with increasing richness (for $f \geq 10$); thus, the random catalogs have essentially no power at large richness. The observed superclusters have systems with more members than seen in the random catalogs for all $f \geq 10$. The observed high-richness superclusters (high $n_{\mathrm{cl/sc}}$) appear to grow rapidly (in richness and size) as f decreases. As these richest, largest scale structures grow, a gap of medium-richness superclusters appears to be rapidly forming (Figure 17). Neither the gap nor the related largest scale structure exists in the random catalogs.

6.3 *Superclusters Surrounding Galaxy Voids*

The BS84 supercluster catalog was used by Bahcall & Soneira (1982a) to study the area around the large ($\sim 60h^{-1}$ Mpc diameter) void of galaxies

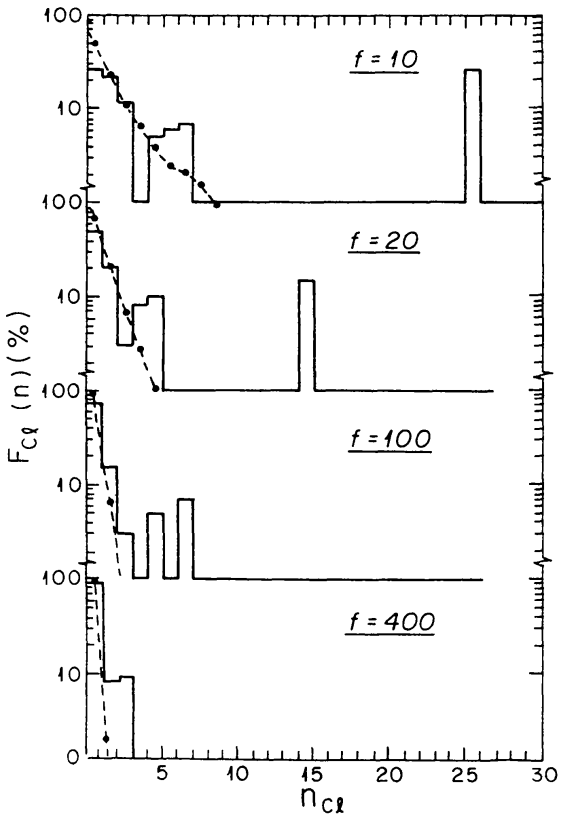

Figure 17 The frequency distribution of $R \geq 1$ clusters that are members of superclusters of various richnesses, $n_{cl/sc}$ (Section 6). (The first bin, $n_{cl/sc} = 1$, refers to single clusters; bins $n_{cl/sc} = 2$, 3, etc., represent superclusters with two, three, etc., cluster members.) The distributions are given for four different density enhancements f. The histogram represents the observed catalog; the dashed line is the average of 100 random catalogs (BS84).

in Bootes that was detected by Kirshner et al. (1981). The largest, densest superclusters are located near and around the area devoid of galaxies. The Bootes void, at approximately $14.5^h + 50°$, is located near superclusters BS 12 and BS 15+16 ($\sim 100h^{-1}$ Mpc away in projection; see Figure 15 and BS84). In addition, the overdensity of galaxies observed by Kirshner et al. (1981) on both redshift sides of the void, at $z \simeq 0.03$ and $z \simeq 0.08$ (Figure 18), coincides in redshift space with these nearby dense superclusters: BS 15+16 (Hercules supercluster) at $z \simeq 0.03$, and BS12 (Corona Borealis supercluster) at $z \simeq 0.08$ (Figure 18). This suggests that the large superclusters surround the galaxy void, and that the tails of their galaxy distributions account for the neighboring overdensities observed $\gtrsim 100h^{-1}$ Mpc away by Kirshner et al. This connection provides another indication of long tails to rich superclusters.

Previous observational evidence (Gregory & Thompson 1978, Gregory et al. 1981, Chincarini et al. 1981), together with these results as well as

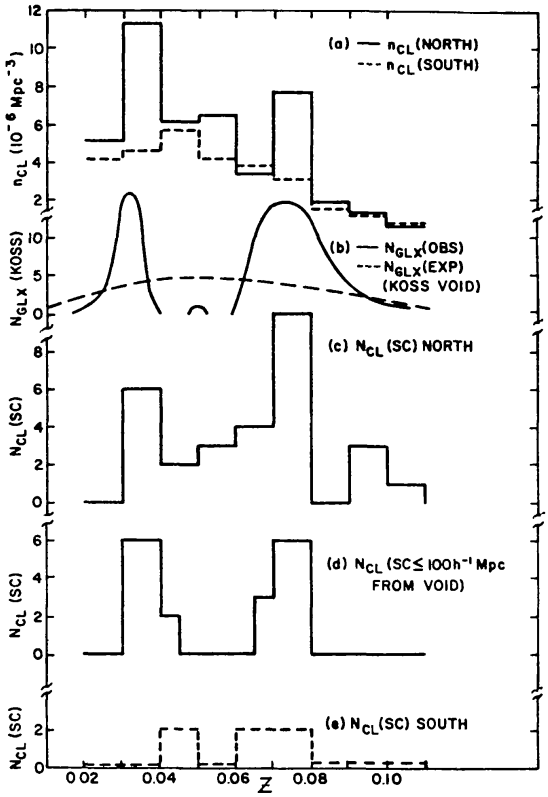

Figure 18 The frequency distribution of Abell clusters, N_{cl}, and galaxies in the Bootes direction (Kirshner et al. 1981), N_{glx}, as a function of redshift. The Bootes void at $z \simeq 0.04$–0.06 and the surrounding galaxy excess at $z \simeq 0.03$ and 0.08 are apparent in (*b*). The $D \leq 4$ cluster distribution in the north (*a*) shows superclustering at the same redshifts as seen in the galaxy excess above (0.03 and 0.08); this superclustering originates close ($\lesssim 100h^{-1}$ Mpc) to the Bootes void (*c*, *d*) at the Hercules supercluster ($z \simeq 0.03$) and Corona Borealis ($z \simeq 0.08$). The tails of these superclusters appear to extend $\sim 100h^{-1}$ Mpc in size and cause the galaxy excess observed around the Bootes void (*b*) (Bahcall & Soneira 1982a).

more recent redshift surveys (Giovanelli et al. 1986, de Lapparant et al. 1986, da Costa et al. 1988), suggests that galaxy voids may generally be associated with surrounding galaxy excesses; the bigger the void, the stronger may be the related excess.

6.4 *Voids of Rich Clusters*

A huge void of cataloged nearby rich clusters of galaxies was suggested by Bahcall & Soneira (1982b) in the complete $D \leq 4$ Abell sample discussed above. The void, located at $l \sim 180°$, $b \sim 30$–$50°$, is in the approximate redshift range of $z \simeq 0.03$–0.08, and it extends $\sim 100°$ across the sky (i.e. $\sim 300h^{-1}$ Mpc). Its projected area is completely devoid of nearby—but not distant—rich clusters ($R \geq 1$). The void does not appear to be caused by absorption in the Galaxy. If this apparent void in nearby rich clusters is real, it subtends a volume of more than $10^6 h^{-3}$ Mpc^3. Simulations with

100 random catalogs indicate that the probability of finding such a large void by chance is $\lesssim 10^{-2}$ [Bahcall & Soneira 1982b; see, however, Politzer & Preskill (1986), who estimate a higher random probability].

Recent work by Lipovetsky (1987), who studied the space distribution of Markarian galaxies from the First Byurakan Survey (using a UV excess technique), indicates a large void in the galaxy distribution in exactly the same rich-cluster void region as was suggested by Bahcall & Soneira (1982b). The cluster catalog of Shectman (1985), which lists poorer clusters than Abell's (Section 2), also has a significant underdensity of poor clusters in this region. Shectman finds 14 poor clusters in this area compared with an expected number of 32 (based on the density of clusters in the same Galactic latitude bin but different longitude). Other large voids in the distribution of rich clusters were suggested by Batuski & Burns (1985b), but no comparisons with random distributions were made. More recently, Huchra (1988) suggested the existence of similar huge voids of clusters using redshift observations of a deep ($z \lesssim 0.2$) subsample of Abell clusters.

Proving that a void exists in a sparse distribution of rich clusters is obviously difficult and can be achieved only for very large regions devoid of clusters. On the other hand, if clusters are observed to be overdense on supercluster scales ($\sim 100h^{-1}$ Mpc), it is reasonable to expect that similar underdense regions exist also.

7. OTHER TRACERS OF LARGE-SCALE STRUCTURE

In the previous sections, I described the use of rich clusters of galaxies as an efficient tracer of the large-scale structure in the Universe. In this section I summarize briefly the use of other tracers of large-scale structure: galaxies, quasars, and microwave background fluctuations. For more details, see the references listed below.

7.1 *Galaxies*

The study of the distribution of galaxies in space has been the classical method of surveying structure in the Universe. Redshift surveys of galaxies, covering either large areas of the sky or narrow and deep "cones," provided important information regarding the structure on scales up to $\sim 20h^{-1}$ Mpc, and, more recently, to larger scales of $\sim 50h^{-1}$ Mpc or more (e.g. Gregory & Thompson 1978, Tarenghi et al. 1980, Einasto et al. 1980, Chincarini et al. 1981, Gregory et al. 1981, Davis et al. 1982, Huchra et al. 1983, Oort 1983, Shanks et al. 1983, Giovanelli et al. 1986, Haynes & Giovanelli 1986, de Lapparent et al. 1986, Chincarini & Vettolani 1987, da Costa et al. 1988, Rood 1988, and references therein). While rich clusters

are efficient tracers of the largest scale structure, galaxies (with their higher space density and smaller mean separation) can better trace the details of smaller and intermediate-scale structures.

The galaxy surveys reveal sharply defined structures of galaxies, frequently surrounding voids or regions underdense in galaxies. A large fraction of the galaxies appear to be located on sheetlike geometries, with occasional high-density filamentary structures such as the Perseus-Pisces supercluster (Giovanelli & Haynes 1982, Giovanelli et al. 1986, Haynes & Giovanelli 1986). The topology of the geometry may be spongy (Gott et al. 1986), i.e. exhibit connected underdense regions ("tunnels") as well as connected overdense regions. The observed voids and overdense regions range in size from a few megaparsecs to a few tens of megaparsecs. Further observations of larger and deeper samples are needed, however, before the topology can be determined more accurately.

The principal *quantitative* measure of the galaxy distribution used so far has been the galaxy correlation function, determined originally by Groth & Peebles (1977) from the angular distribution of galaxies in the Shane & Wirtanen (1967) counts. The galaxy correlation function is expressed by Equation 5. New observational samples yield correlations consistent with this equation (see references above; also Efstathiou 1988). It is of interest to note that while large-scale features of $\sim 50h^{-1}$ Mpc or more are clearly apparent in the redshift surveys, the galaxy correlation function shows no positive correlations on scales larger than $\sim 20h^{-1}$ Mpc. This is in contrast to the cluster correlation function discussed in Section 3; the latter reveals positive correlations on larger scales ($\gtrsim 20h^{-1}$ Mpc). Some additional statistical methods are needed that can express quantitatively the observed morphology of the galaxy distribution.

The study of the galaxy distribution can be extended to high-redshift galaxies (e.g. Koo & Kron 1987). A comparison between the clustering properties of high- and small-redshift galaxies will enable a determination of the evolution of structure with time. This information will provide important constraints on models of galaxy and structure formation.

7.2 *Quasars*

Quasars can provide an important tracer of structure at high redshifts. Since relatively large complete samples of quasars have recently become available, the clustering analysis of quasars has improved. Kruszewski (1986), Shaver (1984, 1988), and Zhu & Chu (1987) have analyzed the spatial distribution of quasars in different large samples. All find significant spatial correlations among quasars to large separations ($\sim 100h^{-1}$ Mpc). They find that quasars with $z \lesssim 1.5$ or 2 are very strongly correlated in space, exhibiting a correlation function that is considerably stronger than

that of galaxies, comparable to the correlations of poor clusters (assuming no evolution; see Section 3). They also suggest that at $z \gtrsim 2$ the correlations weaken considerably and are essentially undetected. Shanks et al. (1987), using a smaller sample of quasars, find strong quasar correlations at small separations ($\lesssim 10h^{-1}$ Mpc) but no significant correlations on larger scales.

The strength and extent of the quasar clustering, and its dependence on redshift, will provide important clues to the understanding of large-scale structure at early times.

7.3 *Microwave Background Radiation*

Another tracer of the universal structure can be provided by the fluctuations in the microwave background radiation. The microwave background is observed to be isotropic to a high degree, reflecting the uniformity of the Universe over all scales at the epoch of recombination ($z \sim 1000$). However, if the present structure in the Universe has grown from seed fluctuations in the early Universe, then a significant level of inhomogeneity must exist in the matter (and radiation) distribution at recombination. For adiabatic models, these fluctuations are expected at the level of $\Delta T/T \simeq 10^{-4}$–$10^{-5}$. Upper limits to the fluctuation amplitude have been obtained by various sensitive experiments in the range $\Delta T/T = 2 \times 10^{-5}$–$3 \times 10^{-4}$ on arcminute scales (Uson & Wilkinson 1984, Lasenby & Davies 1983, Readhead 1988). On large scales of a few degrees (1° corresponds to $\sim 100h^{-1}$ Mpc), Davies et al (1987) have recently reported a possible detection at a level of 5×10^{-5}; if these fluctuations are due to the cosmic background, they would provide evidence for cosmic large-scale structure that is considerably larger than predicted by some current models such as cold dark matter (see Section 9). Further very sensitive observations are currently underway [see, for example, Wilkinson (1988) and Lasenby (1988) for reviews] that should detect (or limit) fluctuations at a level of $\sim 10^{-5}$ on various angular scales and provide a fundamental clue to the existence of structure in the very early Universe.

8. PECULIAR MOTION OF CLUSTERS

The discussion in the previous sections summarizes evidence for the existence of structures on the scale of ~ 10–$150h^{-1}$ Mpc. A question of critical importance is what are the velocity fields in these structures. Peculiar velocities of clusters on these scales may indicate the existence of large amounts of (dark) matter and are of fundamental importance for models of galaxy and structure formation. Early discussions of possible peculiar velocities among clusters in superclusters were presented by Abell (1961) and Noonan (1977). Noonan observed a tendency of clusters with neigh-

boring Abell clusters to have a greater scatter on the Hubble diagram, which was interpreted as a gravitational perturbation on the cluster redshifts due to the neighboring clusters. More recently, Bahcall et al. (1986) used the complete redshift sample of $D \leq 4$ rich Abell clusters (Section 2) to study the possible existence of peculiar motion and/or structural anisotropy on large scales. They find strong broadening in the redshift distribution that corresponds to a cluster velocity of $\sim 10^3$ km s^{-1}. These findings are summarized below.

Recent observations of galaxy peculiar velocities on large scales (Rubin et al. 1976, Dressler et al. 1987, Aaronson & Mould 1988) indicate motion, or a bulk flow, on the scale of approximately $60h^{-1}$ Mpc toward a large mass concentration; the indicated motion is about 600 km s^{-1} relative to the microwave background. Yahil (1988) and Strauss & Davis (1988) used the IRAS galaxy survey to trace the gravitational field over a comparable volume around us. They suggest that velocity flows exist mostly on smaller scales around various local density enhancements (superclusters).

8.1 *Redshift Elongation: The "Finger-of-God" Effect*

The distribution in space of the $D \leq 4$ redshift sample of Abell clusters was studied by Bahcall et al. (1986) by separating the three-dimensional distribution into its components along the line-of-sight (redshift) axis and the perpendicular axes projected on the sky. All clusters were assumed to be located at their Hubble distances as indicated by their redshifts, and their pair separations (in megaparsecs) were determined in the three components. A scatter-diagram of the cluster pair separations in the redshift (z) direction (R_z) versus their separations in α or δ (R_α or R_δ) was then determined.

If all clusters were located at their Hubble distances with negligible peculiar motion, and if the sample was not dominated by elongated structures in a given direction, a symmetric scatter diagram should be observed. If a large peculiar velocity exists among clusters, it would manifest itself as an elongated distribution along the z-direction in the R_z-R_α and R_z-R_δ diagrams. This elongation, often called the "Finger-of-God" effect, is normally interpreted as peculiar motion. However, the effect may also be caused by geometrically elongated structures if they dominate the sample (with elongation in the z-direction; see below).

The results are presented in Figures 19 to 21. The scatter diagrams are plotted in Figure 19 for both the $R \geq 0$ and $R \geq 1$ samples. Frequency distributions representing these diagrams are presented in Figure 21. *A strong and systematic elongation in the z-direction exists in all the real samples studied.* Scatter diagrams for sets of random catalogs do not exhibit any conspicuous elongation (Figure 20), as expected; a symmetric

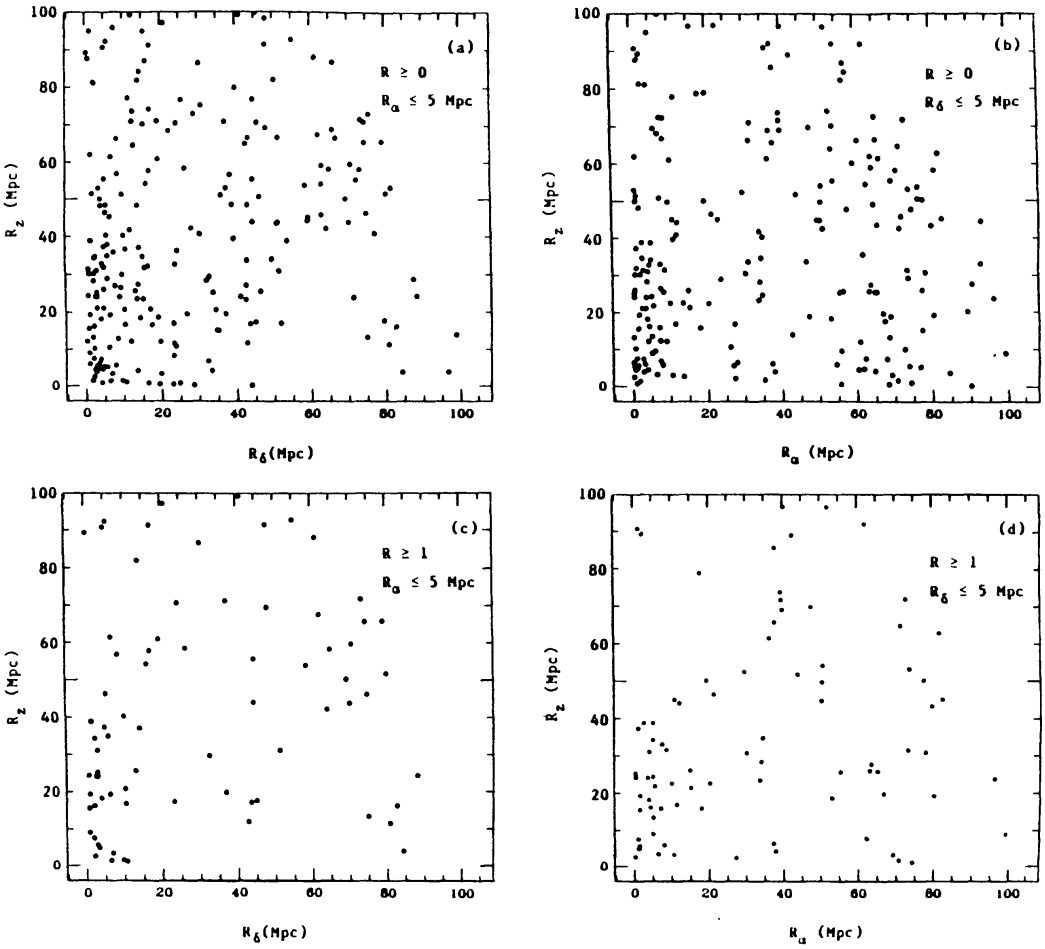

Figure 19 Scatter diagrams of Abell cluster pair separations (in megaparsecs) in the R_z-R_α and R_z-R_δ planes (Bahcall et al. 1986). (The pair separations along the third axis, perpendicular to each plane, are limited to ≤ 5 Mpc.) All cluster pairs with a total spatial separation ≤ 100 Mpc are included. Parts (a, b) and (c, d) represent, respectively, the $R \geq 0$ and $R \geq 1$ richness samples. The elongation in the redshift direction is apparent in all cases (see Section 8).

distribution in all directions is observed. As an additional test, Bahcall et al. (1986) also determined the scatter diagrams in the projected plane R_α-R_δ, of the cluster sample (Figure 20). Again, as expected, a symmetric distribution is observed in this plane. These tests strengthen the conclusion that the observed elongation is real. The effect of elongation is strong; statistically, it corresponds to approximately 8σ in a single sample (assuming, for illustrative simplicity, Gaussian statistics). It is therefore unlikely that the observed redshift elongation is a chance fluctuation. The effect becomes more apparent in the larger $R \geq 0$ sample; *this increase is expected if the effect is real.*

A similar effect was observed by BS83 in their comparison between

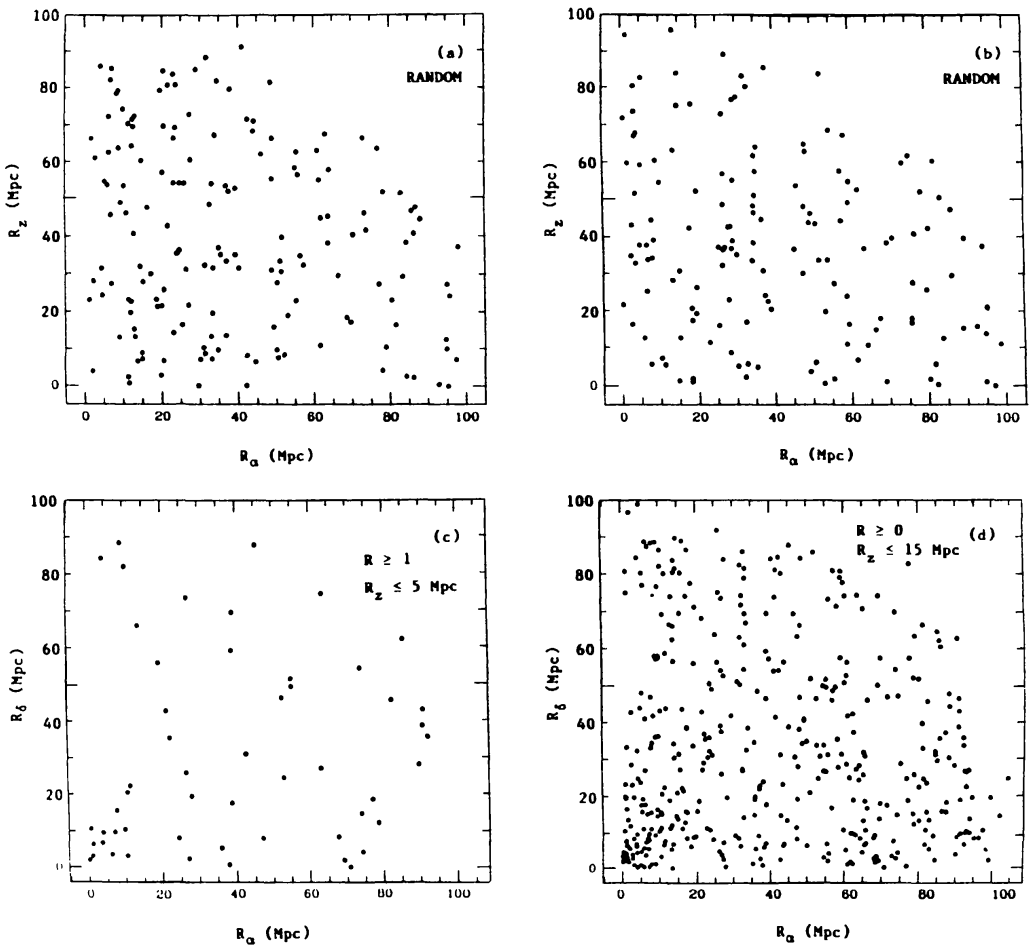

Figure 20 Same as Figure 19 but for typical random distribution of clusters (*a*, *b*), and for the *projected* distribution (i.e. R_δ-R_α plane) of the actual cluster samples (*c*, *d*). No elongation is expected in either case, and none is observed. The clustering of clusters is apparent in the data sample of (*c*, *d*).

the cluster correlation function in the redshift and spatial directions. A broadening in the redshift direction was observed in that study, similar to the present findings. The elongation is unlikely to be caused by background/foreground contamination of galaxies and clusters (e.g. Sutherland 1988), since this would yield an excess of pairs at any R_z separation, as well as any R_α or R_δ, rather than the excess (i.e. broadening) observed specifically at small separations ($\Delta z \lesssim 0.015$). The effect is also much larger than either the uncertainties in the redshift measurements or the uncertainties caused by the internal velocity dispersion within the clusters (see below).

To determine what velocity could cause the observed effect, the authors convolved the frequency distribution observed along the projected axis, which is unperturbed by peculiar motion, with a Gaussian velocity dis-

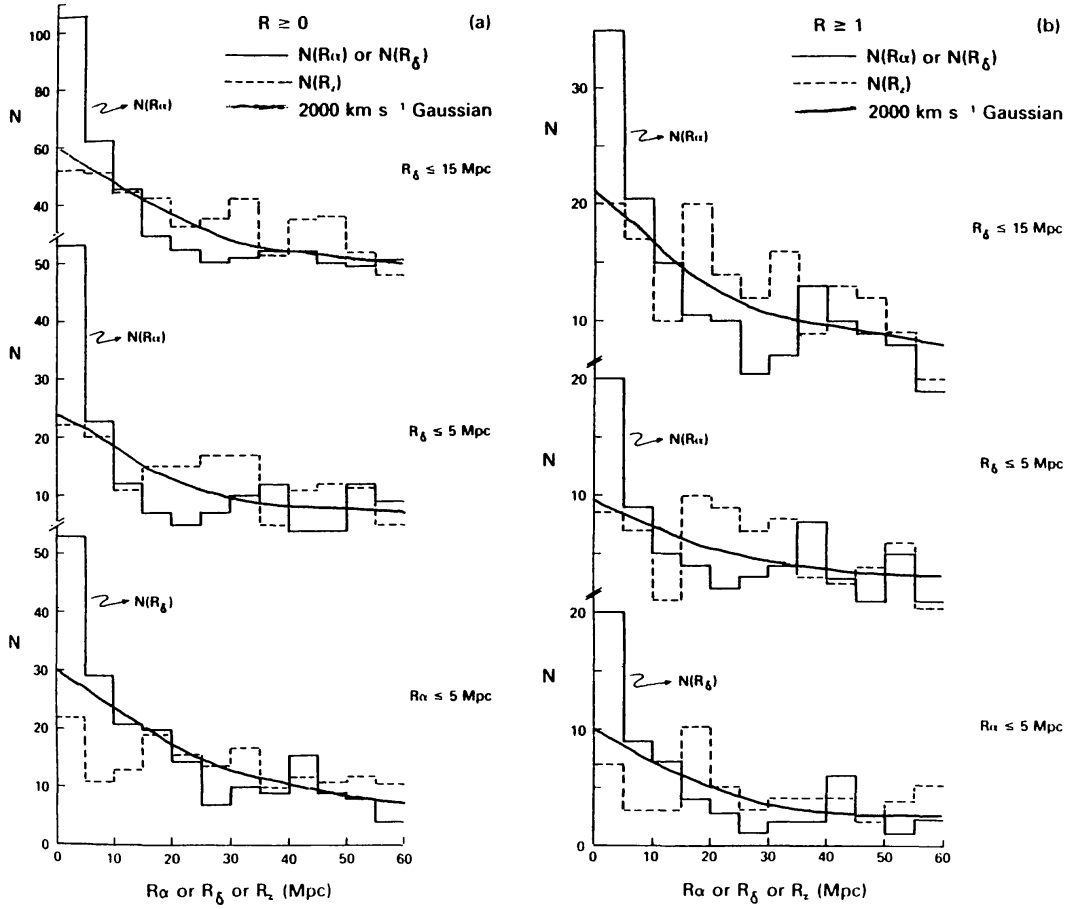

Figure 21 Histograms representing the distribution of pairs along the redshift, R_z, and projected, R_α and R_δ, directions (as determined from the scatter diagrams) are shown for the $R \geq 0$ (*a*) and $R \geq 1$ (*b*) samples. The number of cluster pairs as a function of projected separation, $N(R_\alpha)$ or $N(R_\delta)$, is represented by the solid histogram. The number of cluster pairs in the redshift direction, $N(R_z)$, is represented by the dashed histogram. The solid curve represents a convolution of the projected distribution [$N(R_\alpha)$ or $N(R_\delta)$] with a Gaussian of 2000 km s^{-1} width. This convolved profile is in general agreement with the broadened distribution observed in the redshift direction, $N(R_z)$.

tribution. A Gaussian form is assumed for convenience in estimating the velocity broadening. This convolved distribution should match the broadened distribution observed in the redshift direction. The best fit is obtained for a velocity width of $\sqrt{2}\sigma \simeq 2000$ km s^{-1}. The estimated uncertainty on this mean velocity is approximately $+1000/-500$ km s^{-1}. The above result is consistent with the results of BS83, who used the redshift broadening observed in the cluster correlation function.

The above value for the velocity width includes all contributions to the broadening effect, such as redshift measuring uncertainty and possible deviations from the true cluster redshift due to individual galaxy velocities in the clusters. Redshift measuring uncertainties are negligible compared

with the 2000 km s^{-1} velocity width observed. The effect of peculiar motion within the clusters (for those clusters that have only a small number of measured galaxy redshifts) was estimated by comparing cluster redshifts from the current sample with those obtained using a larger number of measured galaxy redshifts, when available. For the latter study (Bahcall et al. 1986), the redshift catalogs of Sarazin et al. (1982) and Fetisova (1981) were used. A root-mean-square deviation for these cluster redshifts of approximately 300 km s^{-1} is observed due to the above effect. This value is reasonable considering that the full velocity dispersion in clusters is typically $\sim$1000 km s^{-1}, and that the redshifts measured are for the brightest centrally located galaxies; these galaxies are generally close to the central velocity of the cluster. Subtracting quadratically a possible deviation of $300\sqrt{2}$ km s^{-1} from the observed 2000 km s^{-1} yields 1950 km s^{-1}, i.e. a negligible change. Even if we assume, conservatively, $\sim$700 km s^{-1} for the internal broadening, the net cluster pair velocity is still 1740 km s^{-1}. Thus, a considerable elongation effect of approximately 10^3 km s^{-1} per cluster remains after correction for internal motion.

The observed elongation may be caused by either peculiar motion of clusters or a true geometrical elongation of superclusters. These are briefly discussed below.

8.2 *Explanations of the Redshift Elongation*

8.2.1 PECULIAR VELOCITY AMONG CLUSTERS If the observed elongation is caused primarily by peculiar motion of clusters in superclusters, the net cluster pair motion in the line of sight is approximately 1700 km s^{-1}, or, equivalently, about 1200 km s^{-1} for single cluster motion. Most of this effect arises in the central parts of the rich superclusters. A large peculiar velocity could be caused by the gravitational potential of the superclusters or by nongravitational effects such as explosions.

To estimate a supercluster mass that may support this velocity, a typical supercluster size of $\sim 25h^{-1}$ Mpc (=cluster correlation scale length) is used and the virial relation $M \propto v^2 r$ is assumed. This yields a typical supercluster mass of

$$M_{sc} \simeq 2 \times 10^{16}\, M_{\odot}, \qquad r \lesssim 25h^{-1}\ \text{Mpc}. \tag{19.}$$

This mass is comparable to the mass of $\sim$20 rich clusters, while typically only $\sim$3–5 rich clusters are members of a supercluster. Even when the luminous tails of clusters are accounted for, the result may still suggest an excess of dark matter in superclusters as compared with clusters. Using an observed luminosity and/or density profile of r^{-3} or $r^{-2.5}$ around a rich cluster, we estimate an M/L for superclusters that is typically twice that of rich clusters, i.e. $M/L \sim 500$.

Redshift observations of two individual higher redshift superclusters (Ciardullo et al. 1983) appear to indicate a much lower velocity for the superclusters than suggested even by a free expansion. This suggests, for these two systems, either a flat face-on geometry of the superclusters (consistent with Section 8.2.2) or a slow-down of the initial expansion due to the supercluster mass. In either case, it is likely that individual superclusters are at different stages of their evolution as well as at different observed orientations. The Corona Borealis supercluster (Bahcall et al. 1986) appears to show a redshift elongation in the distribution of both its clusters and the galaxies.

8.2.2 GEOMETRICAL ELONGATION OF SUPERCLUSTERS The elongation observed in the scatter diagrams may also be caused, at least partially, by a geometrical elongation of superclusters. If the most prominent superclusters are elongated in the line-of-sight direction, an apparent elongation in the distribution of pair separation along this axis may result. I discuss below an observational test to distinguish between peculiar velocity and geometrical elongation of large-scale structures.

8.2.3 TESTS TO DISTINGUISH BETWEEN PECULIAR VELOCITY AND GEOMETRICAL ELONGATION If the observed redshift elongation is caused by geometrical elongation, cluster redshifts should be correlated with the magnitude of their standard galaxies, following Hubble's law. No such magnitude-redshift correlation should be present if the effect is entirely due to peculiar velocity. More generally, an independent distance indicator (such as the magnitude of the brightest cluster galaxy or Tully-Fisher-type relations) could be used to determine the actual distances to the clusters and thus to interpret the origin of the observed redshift broadening (by comparing the actual distances with the observed redshifts).

The dependence of galaxy magnitudes on redshift in the close cluster pairs was studied by Bahcall et al. (1986). The magnitude of the brightest galaxy in each cluster, m_1^c, corrected for the cluster morphological type and richness as given by Hoessel et al. (1980), was used as a distance indicator. If the observed redshift elongation is caused by geometrical anisotropy, a proper (Hubble) correlation of m_1^c with z is expected within individual superclusters. This correlation should not exist if peculiar velocity is the cause of the observed elongation. The expected magnitude difference for a cluster pair with a redshift separation of about 0.01–0.015, assuming Hubble distances, is $\sim$0.3 to 0.5 mag (depending on z). This difference is large enough to be measured with accurate observations of standard galaxy magnitudes. A marginal m_1^c dependence was found (Bahcall et al. 1986) for some individual superclusters, suggesting that at least some of the redshift broadening observed may be due to geometrical

elongation of the large structures. Increased accuracy and greater statistics for galaxy magnitudes may clarify the significance of the results. It is possible that both geometrical elongation and peculiar velocity of clusters contribute to the observed redshift broadening. Other distance indicators, such as Tully-Fisher or Faber-Jackson relations, should also be applied to the problem in order to help distinguish between peculiar motion and geometry. Recently, comparable velocities of $\sim 10^3$ km s^{-1} between some cluster pairs were also suggested by Mould (1988) and Burstein (1988) using actual distance indicators of galaxies.

9. MODELS

The results on large-scale structure presented above cause difficulties for theories of structure formation when considered together with explanations of the structure on smaller scales (galaxy correlations and properties) and the absence of structure in the microwave background. Both the quantitative measure of the clustering of clusters implied by the strong cluster correlation function, with a correlation scale of $25h^{-1}$ Mpc, and the suggested bulk velocities on large scales are difficult for most current models to explain.

9.1 *Model Parameters*

Before summarizing the status of currently discussed models for the formation of structure, I list some of the fundamental parameters that must be assumed for any model. A number of parameters can be adjusted to fit the observations, but this welcome freedom is also a cause of concern in interpreting the significance of the results.

Some of the free parameters are the following:

1. The value of Ω ($0.2 \lesssim \Omega \lesssim 1$).
2. The value of the cosmological constant Λ ($\Lambda = 0$ or $\neq 0$).
3. The nature of the dark matter (Baryons? Hot dark matter, e.g. $\sim$30-eV neutrinos? Cold dark matter, e.g. axions or $>$ keV photinos? Unstable dark matter? Mixture of some of the above? Note that only the baryons and leptons are currently known to exist).
4. The origin and nature of the initial density fluctuations (Inflation and Gaussian fluctuations? Cosmic strings and non-Gaussian fluctuations? Adiabatic or isothermal? Power-law initial spectrum? What slope?).
5. The effect of nongravitational processes, which may dominate the model (Explosions? Cosmic strings?).
6. Does mass follow the observed light? (or is our basic interpretation of

observations greatly complicated by some kind of biasing? How is it biased?)

Even with the large choice of parameters available, no single elegant model (i.e. one excluding special combinations of particles, fluctuation spectra, or $\Lambda \neq 0$) has yet been proposed that can explain all the observations. Some frustration with available "standard" models motivates new "nonstandard" ideas such as explosions or cosmic strings as a means of explaining the universal structure.

I briefly summarize below the currently available models. For more detailed reviews, see Peebles (1988a,b), Ostriker (1988), White et al. (1987a), Bond (1987), Dekel (1987), Primack et al. (1986), Zeldovich et al. (1982), and references therein.

I divide the models into the following categories:

I. "Standard" Gaussian Fluctuation Models
- Baryonic matter
- Cold dark matter (CDM)
- Hot dark matter (HDM)

II. Non-Gaussian Fluctuation Models
- Cosmic strings

III. Explosions

9.2 *"Standard" Gaussian Fluctuation Models*

9.2.1 BARYONIC MATTER Pure baryonic models of the Universe have not been popular in recent years mainly because of two limitations: the limit imposed on the baryonic mean mass density, $\Omega_b < 0.2$, by standard big-bang nucleosynthesis (e.g. review by Audouze 1987), which would then require an open universe (or, alternatively, the consideration of non-standard nucleosynthesis theories; e.g. Audouze 1987); and the observed isotropy limit of the microwave background, $\Delta T/T < 10^{-4}$ on a 4.5′ scale (Uson & Wilkinson 1984), which implies density fluctuations too small to form galaxies. However, revived ideas of isocurvature fluctuations in an open baryonic universe have been recently considered (Peebles 1987a,b, 1988a) and the model is now fair game for further investigations. The advantages of "What you see is what you get" (i.e. $\Omega \simeq 0.2$ as observed, and only baryons, with no unknown particles) may be more important than the elegance of the solution.

9.2.2 COLD DARK MATTER (CDM) If one requires that $\Omega = 1$ as demanded by inflation, then CDM is the current leading model [although it was hot dark matter (HDM) just a few years ago . . .]. The assumptions in CDM models are simple and are consistent with inflation, and the number of

free parameters is small (White et al. 1987a,b, Blumenthal et al. 1984, and references therein). The model agrees well with observations on small scales when a biased galaxy formation scenario is introduced (Rees 1985, Bardeen et al. 1986, White et al. 1987b, Dekel & Rees 1987). In this scenario, galaxies form only at high-density peaks of the matter distribution, with the galaxy correlation function about 20 times stronger than the underlying mass correlation: $\xi_{gg}(r) \simeq 20\xi_m$. Many observations on small scales can then be matched by a biased CDM model (e.g. galaxy correlation function, flat rotation curves of galaxies, Tully-Fisher-type relations for galaxies, velocities on small scale, number density of galaxy clusters; see references above). The large-scale structure results discussed in this review, however, constitute a difficulty for CDM. Considerable evidence for structure on scales $\gtrsim 30h^{-1}$ Mpc has now been accumulated by a number of investigators; this large-scale structure (and velocity) cannot be matched by unadorned CDM models, which do not produce enough power on large scales ($\gtrsim 20h^{-1}$ Mpc). If these largest scale results are confirmed by new and deeper observations, it will be damaging to the simplest CDM models.

Other testable predictions of CDM include flat rotation curves of galaxies to very large scales ($\sim 0.5h^{-1}$ Mpc) (Frenk et al. 1985), the existence of matter in voids (due to the requirement of a biased galaxy formation process in which matter is considerably less clumped than galaxies), and a highly isotropic microwave background on large scales ($\Delta T/T < 10^{-5}$). Observations of falling rotation curves at scales $\lesssim 0.5h^{-1}$ Mpc, or strong limits on the emptiness of some voids, or a detection of fluctuations $\Delta T/T \gtrsim 10^{-5}$ in the microwave background on large scales [e.g. see Davies et al. (1987) for a possible detection] would also constitute serious difficulties for CDM.

9.2.3 HOT DARK MATTER (HDM) HDM models with matter in the form of massive neutrinos that can account for some of the large-scale structure observations (pancakes, filaments, voids; Zeldovich et al. 1982) were abandoned a few years ago when N-body simulations and analytic models suggested that it would be difficult to form galaxies at high redshifts without overproducing clusters and large-scale structure. However, HDM with antibiasing, i.e. suppressing galaxy formation at high-density regions, may still be a possibility (e.g. Braun et al. 1987), although large peculiar velocities and excessive X-ray emission from massive clusters may still be problems for this model (White et al. 1984).

9.2.4 HYBRID SCENARIOS Hybrid scenarios attempt to combine, in a somewhat ad hoc manner, CDM models on small scales and HDM models on large scales (e.g. Barnes et al. 1985, Dekel 1984, Dekel & Aarseth

1984). In these scenaios, galaxies and large-scale structure may form from different components of the density fluctuation. The model can involve two types of dark matter (baryonic and nonbaryonic) or two types of initial fluctuations (adiabatic and isothermal) [e.g. see Blumenthal et al. (1988) for an open hybrid model with CDM and baryons]. While the hybrid picture may succeed in reproducing several observations on both small and large scales, the number of model parameters is large, and their choice is ad hoc rather than naturally based on first principles.

9.3 *Non-Gaussian Fluctuation Models*

9.3.1 COSMIC STRINGS A rather different method of producing large-scale density fluctuations without producing large thermal fluctuations is the use of non-Gaussian statistics. The recently suggested cosmic strings model (Vilenkin 1985, Albrecht & Turok 1985, Turok 1985) uses the latter to induce the density fluctuations. Cosmic strings are curvature singularities that are born with a topology of random walks. They turn into closed loops, which later break into multiple smaller loops in a scale-free fashion, leading to a scale-invariant fluctuation spectrum. Matter is then accreted onto the loops to form galaxies and clusters. The loop-loop correlation function appears to reproduce the universal correlation function discussed in Section 4, with a power law of r^{-2} (Albrecht & Turok 1985, Turok 1985). This model offers a natural way to account for the large-scale structure observations while keeping a rather isotropic microwave background. More detailed calculations are needed, however, before any conclusions can be reached regarding this model (e.g. Bouchet & Bennett 1988, Turok 1988).

9.4 *Explosions*

A fundamentally different approach to the formation of structure is provided by a model with powerful explosions (Ostriker & Cowie 1981, Ikeuchi 1981). In this model, which is a natural extension of the theory of how some stars form in the interstellar medium, structure is not produced by small density fluctuations in the early Universe but rather from explosions of first-generation objects, which help gravity in forming further galaxies and clusters. The blast waves produced by the explosions push the gas out of an evacuated area; the shells expand, cool, and fragment into a new generation of galaxies. Individual "bubbles" of galaxies formed in this manner, typically of $\sim 10h^{-1}$ Mpc radius, can interact with each other to form clusters, superclusters, and still larger voids (Ostriker 1986). The model predicts a morphological appearance that is indeed similar to that observed in recent galaxy redshift surveys (Section 7). The cluster correlation function can also be reproduced by such a shell model (Bahcall et al. 1988a, Weinberg et al. 1988; Section 5.2). At the same time the

isotropy of the microwave background is preserved, since the structure is formed after decoupling in a way that will not produce significant fluctuations in the background. High peculiar velocities on large scales ($\sim 60h^{-1}$ Mpc) may be a problem for explosions; however, the coherence length of the galaxy velocity field is still under investigation (Section 8). A recent variation on the explosion picture is the use of magnetized superconducting cosmic strings that can give rise to explosionlike phenomena (Ostriker et al. 1986). For recent reviews of the explosion model, see Ostriker (1986, 1988).

10. LOOK TO THE FUTURE

New observational data expected over the next 5 to 10 years will clarify the nature and properties of the large-scale structure. Some of these observations are listed below:

1. Extensive redshift surveys of galaxies over large areas of the sky. These surveys will reveal the shape, type, and extent of structures and voids in the galaxy distribution.
2. Automated deep surveys of clusters of galaxies, including complete samples of X-ray clusters. These surveys will be used to trace the largest scale structures, as discussed in this article.
3. Extensive mapping of the velocity field around us, to larger scales, using various distance indicators.
4. Large samples of high-redshift galaxies, quasars, and quasar absorption lines. These will be available and used as tracers of structure at high redshifts, and the information obtained will help unravel the evolution of structure with time.
5. Very precise measurements of the fluctuations in the microwave background radiation, $\Delta T/T$. These should either detect some anisotropy on large scales or provide a theory-challenging strong limit of isotropy.

The expected observational advances will be of fundamental importance for our understanding of the formation of galaxies and structure in the Universe. Which of the current models will survive, or which new models will be initiated as a result of the new observations, *cannot* be predicted with assurance at this time.

ACKNOWLEDGMENTS

I am grateful to A. Dekel, J. P. Ostriker, P. J. E. Peebles, H. J. Rood, D. Schramm, and A. Szalay for helpful discussions on the topic of this paper. I also express special gratitude to Ray Soneira for the many stimulating and pleasant discussions we had during our collaboration.

Literature Cited

Aaronson, M., Mould, J. 1988. See Audouze & Szalay 1988. In press
Abell, G. O. 1958. *Ap. J. Suppl.* 3: 211
Abell, G. O. 1961. *Astron. J.* 66: 607
Abell, G. O., Corwin, H. G., Olowin, R. 1988. Submitted for publication
Albrecht, A., Turok, N. 1985. *Phys. Rev. Lett.* 54: 1868
Audouze, J. 1987. In *Observational Cosmology, Proc. IAU Symp. No. 124*, ed. A. Hewitt, G. Burbidge, L.-Z. Fang, p. 89. Dordrecht: Reidel
Audouze, J., Szalay, A., eds. 1988. *Evolution of Large-Scale Structure in the Universe, IAU Symp. No. 130*. Dordrecht: Reidel. In press
Bahcall, N. A. 1977. *Ann. Rev. Astron. Astrophys.* 15: 505
Bahcall, N. A. 1979. *Ap. J.* 232: 689
Bahcall, N. A. 1986. *Ap. J. Lett.* 302: L41
Bahcall, N. A. 1987. *Comments Astrophys.* 11: 283
Bahcall, N. A. 1988a. See Audouze & Szalay 1988. In press
Bahcall, N. A. 1988b. See Rubin 1988. In press
Bahcall, N. A., Burgett, W. S. 1986. *Ap. J. Lett.* 300: L35
Bahcall, N. A., Soneira, R. M. 1982a. *Ap. J. Lett.* 258: L17
Bahcall, N. A., Soneira, R. M. 1982b. *Ap. J.* 262: 419
Bahcall, N. A., Soneira, R. M. 1983. *Ap. J.* 270: 20 (BS83)
Bahcall, N. A., Soneira, R. M. 1984. *Ap. J.* 277: 27 (BS84)
Bahcall, N. A., Soneira, R. M., Burgett, W. S. 1986. *Ap. J.* 311: 15
Bahcall, N. A., Henriksen, M. J., Smith, T. E. 1988a. In preparation
Bahcall, N. A., Batuski, D. J., Olowin, R. 1988b. Submitted for publication
Bardeen, J. M., Bond, J. R., Kaiser, N., Szalay, A. 1986. *Ap. J.* 304: 15
Barnes, J., Dekel, A., Efstathiou, G., Frenk, C. S. 1985. *Ap. J.* 295: 368
Batuski, D. J., Burns, J. O. 1985a. *Ap. J.* 299: 5
Batuski, D. J., Burns, J. O. 1985b. *Astron. J.* 90: 1413
Batuski, D. J., Burns, J. O., Laubscher, B. E., Elston, R. J. 1988. Submitted for publication
Blumenthal, G. R., Faber, S. M., Primack, J. R., Rees, M. J. 1984. *Nature* 311: 517
Blumenthal, G. R., Dekel, A., Primack, J. R. 1988. *Ap. J.* 326: 539
Bogart, R. S., Wagoner, R. V. 1973. *Ap. J.* 181: 609
Bond, J. R. 1987. In *Nearly Normal Galaxies*, ed. S. M. Faber, p. 388. New York: Springer-Verlag
Bouchet, F. R., Bennett, D. P. 1988. See Audouze & Szalay 1988. In press
Braun, E., Dekel, A., Shapiro, P. 1987. Preprint
Burstein, D. 1988. See Rubin 1988. In press
Burstein, D., Davies, R., Dressler, A., Faber, S. M., Lynden-Bell, D., et al. 1986. See Madore & Tully 1986, p. 123
Chincarini, G., Vettolani, G. 1987. In *Observational Cosmology, Proc. IAU Symp. No. 124*, ed. A. Hewitt, G. Burbidge, L.-Z. Fang, p. 275. Dordrecht: Reidel
Chincarini, G., Rood, H. J., Thompson, L. A. 1981. *Ap. J. Lett.* 249: L47
Ciardullo, R., Ford, H., Bastko, F., Harms, R. 1983. *Ap. J.* 273: 24
Coles, P. 1986. *MNRAS* 222: 9P
Collins, C. A., Joseph, R. D., Robertson, N. A. 1986. See Madore & Tully 1986, p. 131
da Costa, L. N., Pellegrini, P. S., Sargent, W. L. W., Tonry, J., Davis, M., et al. 1988. *Ap. J.* 327: 544
Davies, R. D., Lasenby, A. N., Watson, R. A., Daintree, E. J., Hopkins, J., et al. 1987. *Nature* 326: 462
Davis, M., Peebles, P. J. E. 1983. *Ap. J.* 267: 465
Davis, M., Huchra, J., Latham, D. W., Tonry, J. 1982. *Ap. J.* 253: 423
Dekel, A. 1984. *Ap. J.* 284: 445
Dekel, A. 1987. In *Observational Cosmology, Proc. IAU Symp. No. 124*, ed. A. Hewitt, G. Burbidge, L.-Z. Fang, p. 415. Dordrecht: Reidel
Dekel, A. 1988. See Rubin 1988. In press
Dekel, A., Aarseth, S. J. 1984. *Ap. J.* 283: 1
Dekel, A., Rees, M. J. 1987. *Nature* 326: 455
de Lapparent, V., Geller, M., Huchra, J. 1986. *Ap. J. Lett.* 302: L1
Dressler, A., Faber, S. M., Burstein, D., Davies, R., Lynden-Bell, D., et al. 1987. *Ap. J. Lett.* 313: L37
Efstathiou, G. 1988. See Rubin 1988. In press
Einasto, J., Joeveer, M., Saar, E. 1980. *MNRAS* 193: 353
Fetisova, T. S. 1981. *Astron. Zh.* 58: 1137
Frenk, C. S., White, S. D. M., Efstathiou, G., Davis, M. 1985. *Nature* 317: 595
Giovanelli, R., Haynes, M. P. 1982. *Astron. J.* 87: 1355
Giovanelli, R., Haynes, M. P., Chincarini, G. 1986. *Ap. J.* 300: 77
Gott, J. R., Mellott, A., Dickinson, M. 1986. *Ap. J.* 306: 341
Gregory, S. A., Thompson, L. A. 1978. *Ap. J.* 222: 784
Gregory, S. A., Thompson, L. A., Tifft, W. G. 1981. *Ap. J.* 243: 411

Groth, E., Peebles, P. J. E. 1977. *Ap. J.* 217: 385
Hauser, M. G., Peebles, P. J. E. 1973. *Ap. J.* 185: 757
Haynes, M. P., Giovanelli, R. 1986. *Ap. J. Lett.* 306: L55
Hoessel, J. G., Gunn, J. E., Thuan, T. X. 1980. *Ap. J.* 241: 486
Huchra, J. P. 1988. See Rubin 1988. In press
Huchra, J. P., Davis, M., Latham, D., Tonry, J. 1983. *Ap. J. Suppl.* 52: 89
Ikeuchi, S. 1981. *Publ. Astron. Soc. Jpn.* 33: 211
Kaiser, N. 1984. *Ap. J. Lett.* 284: L9
Kalinkov, M., Stavrev, K., Kuneva, I. 1984. *C. R. Acad. Bulg. Sci.* 37: 1443
Kalinkov, M., Stavrev, K., Kuneva, I. 1985. *Astron. Nachr.* 306: 283
Kirshner, R. P., Oemler, A. Jr., Schechter, P. L., Shectman, S. A. 1981. *Ap. J. Lett.* 248: L57
Klypin, A. A., Kopylov, A. I. 1983. *Sov. Astron. Lett.* 9: 41
Koo, D. C., Kron, R. G. 1987. In *Observational Cosmology, Proc. IAU Symp. No. 124*, ed. A. Hewitt, G. Burbidge, L.-Z. Fang, p. 383. Dordrecht: Reidel
Kopylov, A. I., Kuznetsov, D. Yu., Fetisova, T. S., Shvartsman, V. F. 1987. *Proc. Semin. Large Scale Structure of the Universe, 1986*, p. 39. Stavropol, USSR: Spec. Astrophys. Obs.
Kruszewski, A. 1986. Princeton Univ. Preprint
Lasenby, A. 1988. See Rubin 1988. In press
Lasenby, A., Davies, R. D. 1983. *MNRAS* 203: 1137
Limber, D. N. 1953. *Ap. J.* 117: 137
Lipovetsky, V. A. 1987. *Proc. Semin. Large Scale Structure of the Universe, 1986*, p. 47. Stavropol, USSR: Spec. Astrophys. Obs.
Maddox, S. J., Efstathiou, G., Loveday, J. 1988. See Audouze & Szalay 1988. In press
Madore, B., Tully, R. B., eds. 1986. *Proc. Conf. Galaxy Distances and Deviations from Universal Expansion.* Dordrecht: Reidel
Mandelbrot, B. B. 1982. *The Fractal Geometry of Nature.* San Francisco: Freeman
Mould, J. 1988. See Rubin 1988. In press
Murray, S. S., Forman, W., Jones, C., Giacconi, R. 1978. *Ap. J. Lett.* 219: L89
Noonan, T. 1977. *Astron. Astrophys.* 54: 57
Oort, J. 1983. *Ann. Rev. Astron. Astrophys.* 21: 373
Ostriker, J. P. 1986. See Madore & Tully 1986, p. 273
Ostriker, J. P. 1988. See Audouze & Szalay 1988. In press
Ostriker, J. P., Cowie, L. L. 1981. *Ap. J. Lett.* 243: L127
Ostriker, J. P., Thompson, C., Witten, E. 1986. *Phys. Lett. B* 180: 231
Peebles, P. J. E. 1980a. *The Large Scale Structure of the Universe.* Princeton, NJ: Princeton Univ. Press
Peebles, P. J. E. 1980b. In *Physical Cosmology, Les Houches Sess. 32*, ed. R. Balian, J. Audouze, D. Schramm, p. 213. Amsterdam: North-Holland
Peebles, P. J. E. 1987a. *Ap. J. Lett.* 315: L73
Peebles, P. J. E. 1987b. *Nature* 327: 210
Peebles, P. J. E. 1988a. *Proc. Conf. The Early Universe*, ed. W. G. Unruh, p. 203. Dordrecht: Reidel
Peebles, P. J. E. 1988b. See Audouze & Szalay 1988. In press
Politzer, H. D., Preskill, J. P. 1986. *Phys. Rev. Lett.* 56: 99
Postman, M., Geller, M., Huchra, J. 1986. *Astron. J.* 91: 1267
Primack, J. R., Blumenthal, G. R., Dekel, A. 1986. See Madore & Tully 1986, p. 265
Readhead, A. 1988. See Audouze & Szalay 1988. In press
Rees, M. J. 1985. *MNRAS* 213: 75P
Rood, H. J. 1976. *Ap. J.* 207: 16
Rood, H. J. 1988. *Ann. Rev. Astron. Astrophys.* 26: 245
Rubin, V. C., ed. 1988. *Large Scale Motions in the Universe, Proc. Vatican Conf., 1987.* In press
Rubin, V. C., Thonnard, N., Ford, W. K. Jr. 1976. *Astron. J.* 81: 719
Sarazin, C. L., Rood, H. J., Struble, M. F. 1982. *Astron. Astrophys.* 108: L7
Sargent, W. L. W. 1988. See Audouze & Szalay 1988. In press
Sargent, W. L. W., Young, P. J., Boksenberg, A., Tytler, D. 1980. *Ap. J. Suppl.* 42: 41
Seldner, M., Peebles, P. J. E. 1977. *Ap. J.* 215: 703
Shane, C. D., Wirtanen, C. A. 1967. *Publ. Lick Obs.* 22: 1
Shanks, T., Bean, A. J., Efstathiou, G., Ellis, R., Fong, R., Peterson, B. A. 1983. *Ap. J.* 274: 529
Shanks, T., Fong, R., Boyle, B. J., Peterson, B. A. 1987. *MNRAS* 227: 739
Shaver, P. 1984. *Astron. Astrophys.* 136: L9
Shaver, P. 1988. See Audouze & Szalay 1988. In press
Shectman, S. 1985. *Ap. J. Suppl.* 57: 77
Shvartsman, V. F. 1988. See Audouze & Szalay 1988. In press
Soneira, R. M., Peebles, P. J. E. 1978. *Astron. J.* 83: 845
Strauss, M. A., Davis, M. 1988. See Audouze & Szalay 1988. In press
Strukov, I. A., Skulachev, D. P., Klypin, A. A. 1988. See Audouze & Szalay 1988. In press

Sutherland, W. 1988. Submitted for publication
Szalay, A. S., Schramm, D. N. 1985. *Nature* 314: 718
Szalay, A. S., Hollosi, J., Toth, G. 1988. Preprint
Tarenghi, M., Chincarini, G., Rood, H. J., Thompson, L. A. 1980. *Ap. J.* 235: 724
Thuan, T. X. 1980. In *Physical Cosmology, Les Houches, Sess. 32*, ed. R. Balian, J. Audouze, D. Schramm, p. 277. Amsterdam: North-Holland
Tully, R. B. 1986. *Ap. J.* 303: 25
Tully, R. B. 1987a. *Ap. J.* 321: 280
Tully, R. B. 1987b. *Ap. J.* 323: 1
Turok, N. 1985. *Phys. Rev. Lett.* 55: 1801
Turok, N. 1988. See Audouze & Szalay 1988. In press
Uson, J., Wilkinson, D. T. 1984. *Ap. J.* 283: 471
Vilenkin, A. 1985. *Phys. Rep.* 121: 264
Weinberg, D. H., Ostriker, J. P., Dekel, A. 1988. Preprint
White, S. D. M., Davis, M., Frenk, C. S. 1984. *MNRAS* 209: 27P
White, S. D. M., Frenk, C. S., Davis, M., Efstathiou, G. 1987a. *Ap. J.* 313: 505
White, S. D. M., Davis, M., Efstathiou, G., Frenk, C. S. 1987b. *Nature* 330: 452
Wilkinson, D. 1988. See Audouze & Szalay 1988. In press
Yahil, A. 1988. See Rubin 1988. In press
Zeldovich, Ya. B., Einasto, J., Shandarin, S. F. 1982. *Nature* 300: 407
Zhou, Y. Y., Fang, D. P., Deng, Z. G., He, X. T. 1986. *Ap. J.* 311: 578
Zhu, X., Chu, Y. 1987. Preprint
Zwicky, F., Herzog, E., Wild, P., Karpowicz, M., Kowal, C. T. 1961–1968. *Catalog of Galaxies and Clusters of Galaxies*, Vols. 1–6. Pasadena: Calif. Inst. Technol.